

Design of a Formula Student race car chassis

Jannis D.G. van Kerkhoven, 516303

DCT 2008.154

Master's thesis

Coach: Piet van Rens
Vision Dynamics B.V.

Supervisor: Prof. dr. ir. M. Steinbuch
Eindhoven University of Technology

Technische Universiteit Eindhoven
Department Mechanical Engineering
Dynamics and Control Technology Group

Eindhoven, December, 2008

*"Adding power makes you faster on the straights,
subtracting weight makes you faster everywhere."*

- Anthony Colin Bruce Chapman -

Founder of the British sports car company Lotus

Abstract

The design of race car for the Formula Student competition involves more performance parameters than for regular racing. In addition to achieving high strength and stiffness for a very low overall weight, the car must be easily manufacturable and maintainable to stay within budget. In this report an approach is presented on designing a lightweight hybrid race car chassis consisting of a fiber reinforced composite cockpit combining structural, esthetic, ergonomic and crash properties, and a tubular space frame engine compartment, meeting stiffness and strength demands while remaining easy to maintain and manufacture, thus keeping production cost low.

Preface

July 2008: the University Racing Eindhoven team heads for the Silverstone circuit to enter the Formula Student competition in great anticipation and hungry for success. Fifty men and a women strong, the basecamp is set up and the final preparations are completed. Amongst this large team, a small band of outlaws roam freely through the paddock and they have their minds set on winning. Undistracted by all the heavy pondering on the track and the pure chaos of the pitlane they are heading for the ultimate prize: the overall Class 3 Award for best design concept.

As the moment of truth approaches the tension rises to an unknown level. The cost reporting is up first: the professionalism radiates from the large flat screen while sheets concerning cost management strategies and flow charts of strategic planning dazzle the judges. Notes are made for implementation at their own employers while our manufacturing specialist comes up with cost efficient techniques and processes they never even heard of!

One down, two more to go, the technical quality of the concept must be accounted for next: the engine specialist has a jungle of hair held up straight by the engine grease from his hands from a long night of work while the Constant Variable Transmission rests enlightened on her pedestal accompanied by the stereo-lithographic chassis model. The judges closely investigate the ideas and their technical justifications, the motives, the drive, the team spirit and they are impressed. First place!

The final run for victory is set in motion as the team manager and his loyal accomplice head for the stands to roll out the red carpet and sell the concept to potential investors with a plan that involves millions of euro's. "Great enthusiasm", "Very professional", "The best question and answer session yet", "Well done guys!!"

Slowly the dust, thrown up by hundreds of feet driven by the adrenaline of intense competition, settles, as all teams pack their bags. University Racing Eindhoven has done what it came to do: it won!!

During my final thesis, I've had the unique opportunity to be responsible for the team's entry in the Formula Student race car design competition. We won the awards for best technical design as well as the overall ranking. Many thanks are owed to all the people involved, some of them briefly, others for years, for their help, their advice, their support, their feedback, their teaching and the many, many laughs.

Jannis van Kerkhoven
Eindhoven, december 2008

Contents

Abstract	ii
Preface	iii
1 Introduction	I
1.1 Formula Student: The Challenge	1
1.2 Problem Definition	2
1.3 Design Approach	3
2 Design Specification	4
2.1 Formula SAE rules	4
2.2 Stiffness	4
2.3 Structural strength	7
2.4 Low or lightweight?	9
2.5 Manufacturability	10
2.6 Ergonomics	10
3 Loads on the chassis	II
3.1 Hardpoint load	12
3.2 Torsional load	13
3.3 Front impact load	13
4 Overview of used materials	I4
4.1 Fiber Reinforced Plastics	14
4.2 Core materials	19
4.3 Core insert materials	20
4.4 Tube materials	21

Contents

4.5	Global laminate stiffness	22
4.6	Global ply failure	25
4.7	Laminate design consideration	26
4.8	Local ply failure	26
4.9	Insert design consideration	29
5	General structural considerations	32
5.1	Torsional stiffness	32
5.2	Bending stiffness	35
5.3	Multi-Shell Assembly Approach	36
5.4	Tubular rear frame	37
6	Ergonomics	38
7	Final design	41
8	Stiffness and strength analysis	45
8.1	Torsional stiffness	45
8.2	Specific stiffness	48
8.3	Stress peaks due to geometrical inefficiencies	49
8.4	Eigen mode analysis	50
8.5	Hardpoint analysis	53
8.6	Rear frame tension and buckling	65
8.7	Front impact equivalency	66
8.8	Side impact/front roll hoop bracing equivalency	67
9	Conclusions and Recommendations	68
Appendix A	Why lightweight?	70
A.1	The downside of load transfer	70
A.2	Low and lightweight	73
Appendix B	Cockpit regulations	75

Chapter 1

Introduction

1.1 Formula Student: The Challenge

University Racing Eindhoven (URE) is a racing team ran by and consisting of students, mainly from the Eindhoven University of Technology. Each year the team designs, builds, tests and eventually races their car against other university teams from all over the world in the Formula Student competition.

The students are to assume that a manufacturing firm has engaged them to produce a prototype car for evaluation. The intended sales market is the non-professional weekend autocross or sprint racer, and the firm is planning to produce 1,000 cars per year at a cost below EURO 21.000.

The car must be low in cost, easy to maintain, and reliable, with high performance in terms of its acceleration, braking, and handling qualities. Watched closely by industry specialists who volunteer their time each team will go through the following rigorous testing process of their car:

Static events:

- Design, Cost and Presentation Judging
- Technical and Safety Scrutineering
- Tilt Test to prevent cars rolling over
- Brake and Noise Test

Dynamic Events:

- Skid Pad (Figure of 8)
- Acceleration
- Sprint/qualification
- Endurance and Fuel Economy

1.2 Problem Definition

A typical open wheeled single seater chassis in the Formula Student competition consists of several parts:

- a lightweight structural and protective driver compartment or cockpit
- a lightweight structural engine compartment
- esthetic and aerodynamic exterior
- crash impact attenuators

So far the team has been building the cockpit using aluminum honeycomb sandwich panels [19]. These panels have a very high stiffness to weight ratio, or specific stiffness, and are fairly cheap. However to use them correctly in a race car is very difficult because they offer very little design freedom. Problems are met when trying to attach the advanced suspension system to the structural cockpit. Additional material is required to meet stiffness and strength demands which partly cancels the advantage of the lightweight panels. The necessary addition of material increases the material cost and the increase in vehicle mass and center of gravity height reduces performance in handling.

In the past the team has constructed the engine compartment from these sandwich panels as well. This resulted in problems with heat dissipation from the engine and great difficulty reaching parts. This reduced the maintainability severely and, because of difficult maintenance and overheating, the reliability. Last year a change was made constructing the engine compartment from a steel tubular space frame. A trade-off was made to increase maintainability and reliability at the cost of additional mass. An additional benefit was the straightforward manufacturing and assembly.

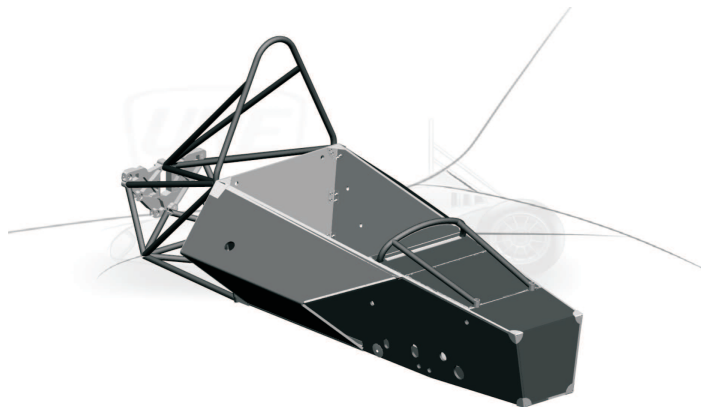


Figure 1.1: Former design of a URE hybrid chassis using aluminum honeycomb panels and a tubular space frame

The esthetics and aerodynamics of the car consisted so far of separate body panels that were basically 5 kg's worth of stickers. In manufacturing these body panels the team gained its first experience with carbon fiber reinforced plastics.

The team has seen the advantages of carbon fiber reinforced plastics (cfrp's) in structural parts of a race car chassis. They offer superb specific stiffness and strength characteristics and great design freedom. Parts made from cfrp's however are often difficult to manufacture and very costly regarding materials. The challenge then is to find a way of applying these high end materials in such a way that an easy manufacturing process reduces the production complexity and thus the cost.

The crash impact system is found mainly at the front of the car. Tight regulations determine maximum decelerations and minimal dimensions. In the past a foam crash cone glued to a thick obligatory anti-intrusion plate was bolted to the chassis to meet these demands.

The engine department is still to be constructed as a open space frame. It can be severely optimized however to form a strong, simple and yet lightweight rear frame.

Using the design freedom of the cfrp's, the esthetic and aerodynamic exterior can be integrated in the structural driver compartment as well as possible crash impact properties. Regarding the relatively low speeds in the competition aerodynamics are less important. Drag resistance reduction and underbody effects can be used to further improve the cars performance. These are outside the scope of this report however and are researched separately to improve future designs. The detailed design and testing of the front crash impact, being the nose cone, is done separately as well.

Summarizing the above, the challenge becomes: *Design a lightweight hybrid race car chassis consisting of a fiber reinforced composite monocoque combining structural, esthetic, ergonomic and crash properties, and a tubular space frame engine compartment, meeting stiffness and strength demands while remaining easy to maintain and manufacture, thus keeping production cost low.*

1.3 Design Approach

To achieve a high quality design the following approach is used:

- The design specifications that follow from the problem definition are stated
- The loads that act on the wheel centers of a Formula Student car have been analyzed previously by Lamers [15] and are used to evaluate the quantity and quality of the different loads that act on the chassis
- The structural possibilities and limitations regarding the available materials are investigated
- The structural engineering aspects regarding a lightweight though stiff and strong and easy to manufacture design are presented
- Ergonomic and safety issues are evaluated
- All these factors are then combined in the final design that has been found iteratively using extensive FEA techniques

Chapter 2

Design Specification

The performance is off course the main issue in designing a race car. In the Formula Student competition the biggest advantage over the competition is achievable through superior handling of the vehicle, or lateral grip. Besides the mass of a vehicle there are a number of parameters that influence the vehicle handling are discussed below.

In the Formula Student competition performance is not the only important design parameter however. The car has to be built by untrained students with a relatively small budget. So the chassis must meet the design specifications at all time while remaining simple and straightforward to built.

What the team lacks in funding and extensive experience in composites it makes up for in cheap and abundant labor and knowledge.

2.1 Formula SAE rules

Every race car competition has an extensive set of rules to provide the necessary safety and to prevent the competition from becoming unfair. There's a number of very strict rules that have to be taken into account in designing the chassis for the UREo9, manly with respect to safety issues. These rules are explained throughout the report when decisive for the design.

2.2 Stiffness

The most important performance measure for a race car chassis is the hub-to-hub torsional stiffness (see Figure 2.1). To find an optimum in suspension setup, the smallest variation in front and rear anti-roll stiffness should be felt immediately by drivers. To ensure this, high torsional rigidity of the chassis with respect to the anti-roll stiffness is required.

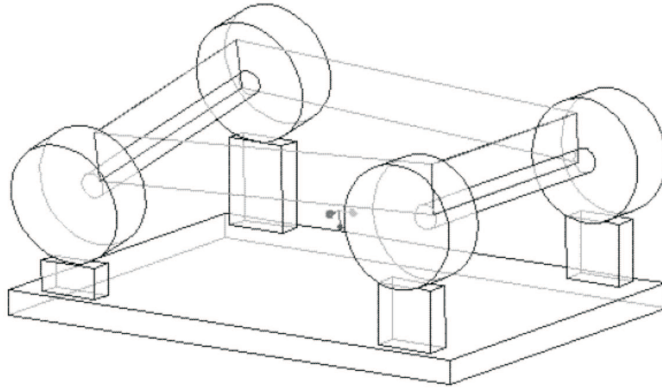


Figure 2.1: The most important bending mode of a race car chassis, longitudinal torsion [12]

Another important factor is the influence of chassis torsional stiffness on the lateral load transfer balance between the front and rear wheels. An example is presented to illustrate this:

When the car enters a corner the steering wheel is turned, this means that, at this instant, the front wheels generate lateral force because, while the rear wheels don't do anything yet. This lateral force at the front wheels is inherently connected to load transfer from the inner to the outer wheel (see Appendix A). Let's assume a point mass on the front wheels m_f and one on the rear m_r with the chassis torsional stiffness connecting them. When the front wheels experience lateral force due to the steering wheel angle, the mass m_f experiences a lateral acceleration causing the mentioned load transfer. Note hereby that for masses higher than the road surface lateral grip cannot exist without load transfer [?]. If the chassis torsional stiffness is very small the rear wheels don't feel any load transfer yet - it takes a while before the car enters the corner properly and the rear mass starts feeling lateral acceleration as well causing load transfer and thus lateral grip. This means that together with the mass distribution over the front and rear wheels the torsional stiffness determines the distribution of dynamic lateral load over the front and rear wheels. Because load transfer and thus lateral grip also inherently decreases the lateral grip that the tires can deliver (see Appendix A) the dynamics of the lateral load transfer and thus the chassis torsional stiffness has an influence on the under or oversteering character of the car. Deakin *et al* [3] have shown that cars with low torsional chassis stiffness are mostly understeered. Considering understeered behavior is already a problem for the most Formula Student cars, a high torsional rigidity is desirable.

Different approaches exist to estimate a target for the specific torsional stiffness [12]. In general targets are varied from 2-10 times the roll stiffness. The URE05 is fitted with an anti-roll stiffness of about 50 kNm/rad front and rear. The highest chassis stiffness in the competition is for a full monocoque structure being approximately 300 kNm/rad weighing little over 20 kg's (Bayreuth's FR8 Chromo). The competition average stiffness lies around 140 kNm/rad for an average chassis

weight of 25 kg . So 3-6 times the anti-roll stiffness seems a more realistic target, Deakin *et all* state a factor of 4 is sufficient for Formula Student cars.

Very high stiffness is usually achievable, though at a severe weight penalty, thus the stiffness per kilogram chassis - or specific stiffness - is a more appropriate measure. In addition, increasing the chassis stiffness is not very effective above a certain value. To illustrate this we model the car as three torsion tubes in series (see Figure 2.2); a front and rear tube representing the suspension system stiffness in torsion k_{susp} and one for the chassis with stiffness $k_{chassis}$. Their respective stiffness can be added up to represent the total vehicle resistance to torsional deflection k_{veh} . To make it more clear k_{veh} is then divided by the total suspension stiffness to indicate the stiffness relative to the rigid case.

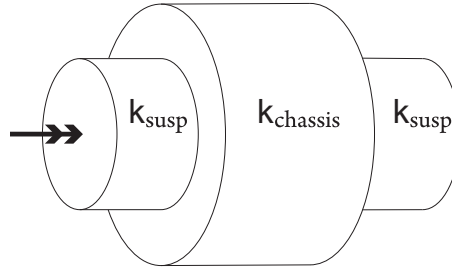


Figure 2.2: Simplified model of the suspension and chassis torsional stiffness

$$\begin{aligned} \frac{1}{k_{veh}} &= 2 \cdot \frac{1}{k_{susp}} + \frac{1}{k_{chassis}} \\ k_{rel} &= \frac{k_{veh}}{2/k_{susp}} \end{aligned} \tag{2.1}$$

Assuming the resistance to torsion by the suspension front and rear is represented by the anti-roll stiffness (50 kNm/rad front and rear) we can plot the total vehicle stiffness as a function of the chassis stiffness (Figure 2.3). It is clear that upwards of 90% of the rigid case, about 4 times the anti-roll stiffness, it becomes less interesting to pay an increasingly large weight penalty for only slight improvements in vehicle stiffness.

Considering the team has a hybrid chassis a trade-off is made between achievable stiffness, weight and manufacturability and maintainability. The target for the chassis stiffness is set to at least 4 times the anti-roll stiffness and well above the competition average.

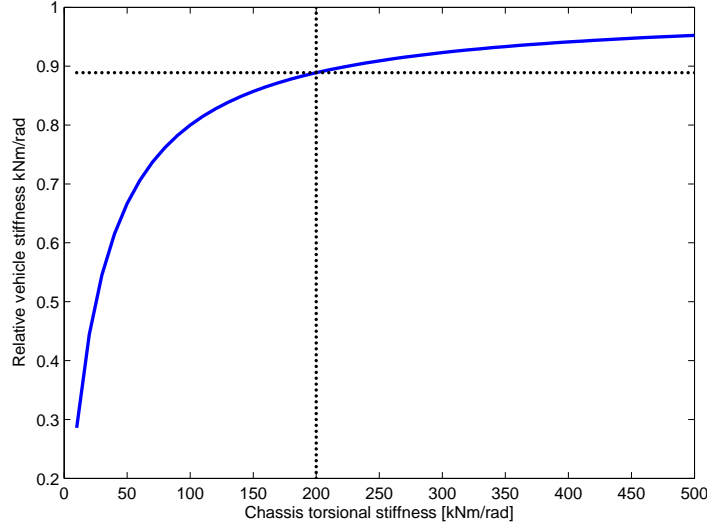


Figure 2.3: Effect of increasing the chassis stiffness at a severe weight penalty on the total vehicle stiffness relative to the rigid case

	mass	stiffness	specific stiffness
Competition low	30 kg	50 kNm/rad	1.7 kNm/rad/kg
Competition average	25 kg	120 kNm/rad	4.8 kNm/rad/kg
Competition high	20 kg	300 kNm/rad	15 kNm/rad/kg
URE05 chassis	<25 kg	>200 kNm/rad	>8 kNm/rad/kg

Table 2.1: Current status of torsional stiffness in Formula Student race cars

2.3 Structural strength

The chassis has to withstand the loads from the suspension system and reactional forces from the driver and the engine. These loads are presented in Chapter 3. For the structural driver compartment the hardpoints are critical, the force interface points on the CFRP monocoque. Furthermore no stress peaks may occur due to geometrical inefficiencies (sharp angles in load paths for instance). Regarding the rear frame, tension and buckling limits in the frame members are analyzed.

Among other requirements, the vehicles structure must include two roll hoops that are braced (main and front), a front bulkhead with an impact attenuator, a driver restraint harness and side impact structures. These crash safety features add structural demands to the chassis. The corresponding parts of the monocoque chassis must be equivalent to a steel tubular structure in yield and ultimate strengths in bending, buckling, and tension. The main roll hoop with its bracing must always be built out of steel tubes, as well as the front roll hoop. For the other parts the equivalent steel tubular minimal dimensions are shown in Table 2.2. The side impact structure in tubular form, as well as the roll hoops are shown in Figure 2.3.

Component	Outer diameter x wall thickness
main and front roll hoops shoulder harness mounting bar	25.0 x 2.50 mm or 25.4 x 2.40 mm
Side impact structure, front bulkhead, roll hoop Bracing, driver restraint harness attachment	25.0 x 1.75 mm or 25.4 x 1.60 mm
Front bulkhead support	25.0 x 1.50 mm or 25.4 x 1.25 mm or 26.0 x 1.20 mm

Table 2.2: Minimum mild steel tubular dimensions the monocoque must be equivalent to

The front impact attenuator must be fixed to the front bulkhead of the monocoque so that it is equivalent to a regular steel tubular frame front bulkhead support. From the rules it follows that the chassis must be able to withstand a static force of 120 kN.

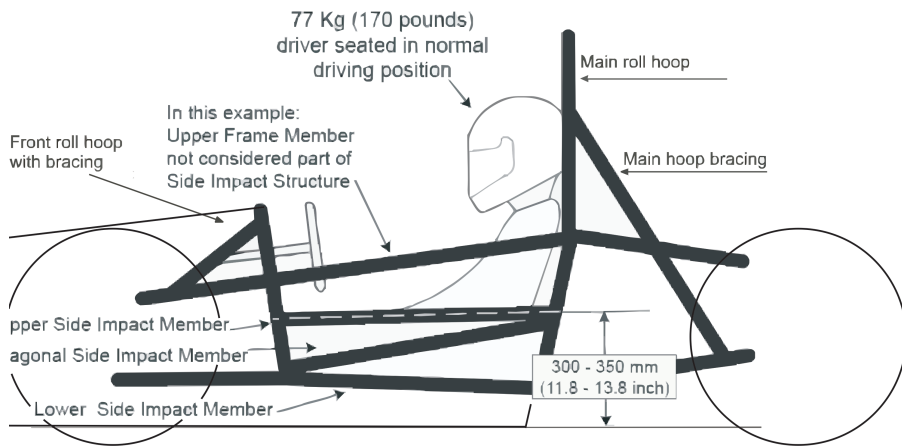


Figure 2.4: Monocoque side impact strength must be equivalent to a certain steel space frame [1]

2.4 Low or lightweight?

Lamers [15] has investigated the sensitivity of lateral grip in g's to both the overall mass in kg's and the center of gravity height in cm's. He came up with a two convenient numbers to indicate these sensitivities respectively:

Lateral g's to mass	$2.49 \cdot 10^{-3} [g][kg]^{-1}$
Lateral g's to COG height	$11.75 \cdot 10^{-3} [g][cm]^{-1}$

Table 2.3: Sensitivity of lateral grip to total vehicle weight and CG height

Lamers states that physically lowering the mass has about five times the effect on vehicle handling than lowering the mass numerically. However the sensitivity for CG height is measured in centimeters. Now considering the UREo4 has a center of gravity height of approximately 280 mm (including the driver) weighing a formidable 240 kg's. The orders of magnitude for these parameters are quite similar so perhaps these sensitivities would make much more sense if stated in $[g][kg]^{-1}$ and $[g][mm]^{-1}$. Then lightweight design would become more interesting to increase lateral grip. In Appendix A is explained more thoroughly how the total mass and center of gravity height influence the lateral grip.

According to the drivers that have been interviewed, the UREo4 has good handling characteristics. Looking at the possibilities, the center of gravity can be lowered further by changing the drivers seating position. By decreasing the angle of the drivers back with the horizontal his center of gravity is lowered. In addition this would allow for a lower main roll hoop (this is more thoroughly explained in Chapter 6). The total vehicle weight can be lowered by using the design freedom of the CFRP's to reduce the additional material that has to be added to the structural driver compartment to meet stiffness and strength demands. In addition more parts can be integrated in the design such as the head rest and the dashboard.

The only real indication that can be given is, improve with respect to last years car. Lower both the vehicle weight and center of gravity height. In a previous paragraph a mass limit for the chassis has already been set to <25 kg's (much lighter then the UREo4) and the CG height of the chassis should be as low as possible.

2.5 Manufacturability

The cost aspect is very important for the team to be able to actually built the chassis but even more so the technical skill that is required to do so. The material and tooling cost must be kept low. This makes it easier for the team to find sponsors. The complexity must be limited to allow the team to built the chassis themselves using the available labor to further reduce manufacturing costs for the team.

This means for the monocoque: Use as few molds as possible without compromising the required design freedom. And for the steel rear frame: A simply weldable rear frame.

2.6 Ergonomics

One of the most determining factors in the competition is the driver. The driver can be aided in his performance by ensuring that all controls can be easily reached, he has a comfortable seating position and that visibility over the front of the chassis is sufficient. Besides being comfortable the driver must be safe at all times. In addition to the structural demands with respect to crash safety, there are some tight geometrical regulations regarding the cockpit to keep the driver safe. This involves mainly dimensional demands for the cockpit to allow for quick driver egress in case of accidents (Appendix B) and the roll hoops that surround the driver. These roll hoop regulations are often with respect to a so called 95th percentile male. This is a statistical representation meaning that at least 95 percent of the male population must be able to drive the car safely (dimensions given in Chapter 6).

Chapter 3

Loads on the chassis

As mentioned in Chapter 2 the main loads on the chassis are from the suspension system and reactional forces of the driver and engine (the main masses) to the lateral longitudinal and vertical accelerations. The suspension geometry that has been designed is shown, as well as the positions of the driver and engine. The definition of the different rods is shown and the major force directions are indicated. Important is that the connection rod forces are merely push and pull forces due to an advanced multi-link system.

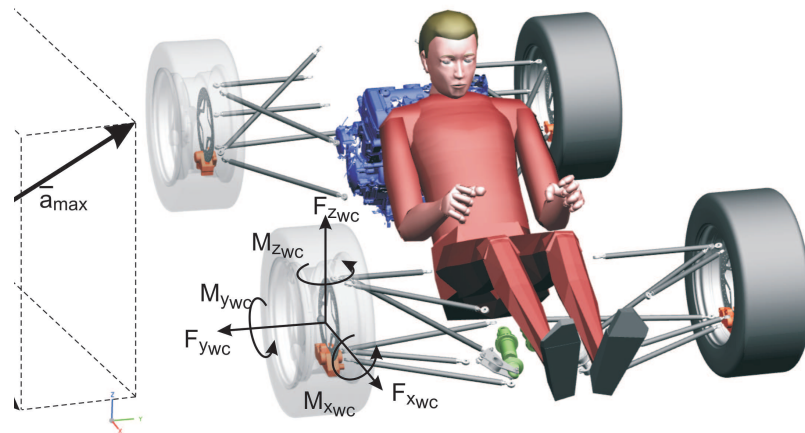


Figure 3.1: The suspension geometry, main accelerations a_x , a_y and a_z and front right tire forces F_x , F_y and F_z

During the design of the suspension system by Lamers [15], a virtual reality analysis has been completed to give good estimations of the dynamic forces F_x , F_y and F_z that occur in the tire road contact patch. These are translated to the forces and moments in the wheel center (*wc*) using the mechanical and pneumatic trails (*t* and *c*) and the *wc* height. An analyses has been made for maximum acceleration/braking, cornering with 70 km/h and a bump manoeuvre driving over a 40x40 mm obstacle. On-track measurements are currently in development to ver-

ify the simulations. These are however not finished on the time of writing. A worst case scenario of cornering with 70 km/h, full braking and hitting a bump is used to evaluate the maximum forces and moments at the front right wheel center, where the largest forces occur in a left corner. The brake and bump forces are added to the cornering forces (Table 3). Directions are defined as shown in Figure 3.

	cornering	braking	bump	Total	
$F_{x_{wc}}$	≈ 0	-1750	-200	-1950	N
$F_{y_{wc}}$	-2450	≈ 0	≈ 0	-2450	N
$F_{z_{wc}}$	1300	+500	+2500	4300	N
$M_{x_{wc}}$	700	≈ 0	≈ 0	700	Nm
$M_{y_{wc}}$	≈ 0	+500	56	556	Nm
$M_{z_{wc}}$	-10	≈ 0	-10	-20	Nm

Table 3.1: Front right wheel center forces for a left corner

Reactional forces from the engine and driver are determined by the maximum longitudinal, lateral and vertical accelerations a_x , a_y and a_z . Both longitudinal and lateral accelerations are limited by the maximum coefficient of friction of the tyres. Extensive tire analysis shows 1.55 g in both directions to be a maximum (reference not yet available). Riley et al [12] found vertical accelerations of 3.5 g to be the maximum bump acceleration on Formula Student tracks. Simple vector calculation shows that the maximum acceleration for any mass in the vehicle is:

$$\bar{a}_{max} = g \cdot \sqrt{2 \cdot 1.55^2 + 3.5^2} \approx 4g \approx 40 \text{ m/s}^2 \quad (3.1)$$

3.1 Hardpoint load

To determine the maximum hardpoint force, the suspension forces and reactional forces are compared.

Firstly lets assume the driver, the largest mass, is suspended in the monocoque from a single point. A maximum acceleration of 40 m/s² for a 70 kg driver would result in a maximum force of approximately 2.8 kN, stated that this is already a very unrealistic situation.

Looking at the worst case scenario mentioned above - i.e. adding the maximum force of braking, cornering and bump - an FEA model is used to calculate the reactional forces in the connection rods. The wheel and upright are modeled as rigid and the connection rods are 3 DOF connected to the chassis, simulating ball joints. The stresses in N/mm² in the rods are simulated and shown in Figure 3.1. Considering the connection rods have a surface of $\approx 70 \text{ mm}^2$ the maximum force for the worst case scenario is approximately 5.6 kN.

Considering both these situations a hard point load of 10 kN is used in the strength analysis of Chapter 8.

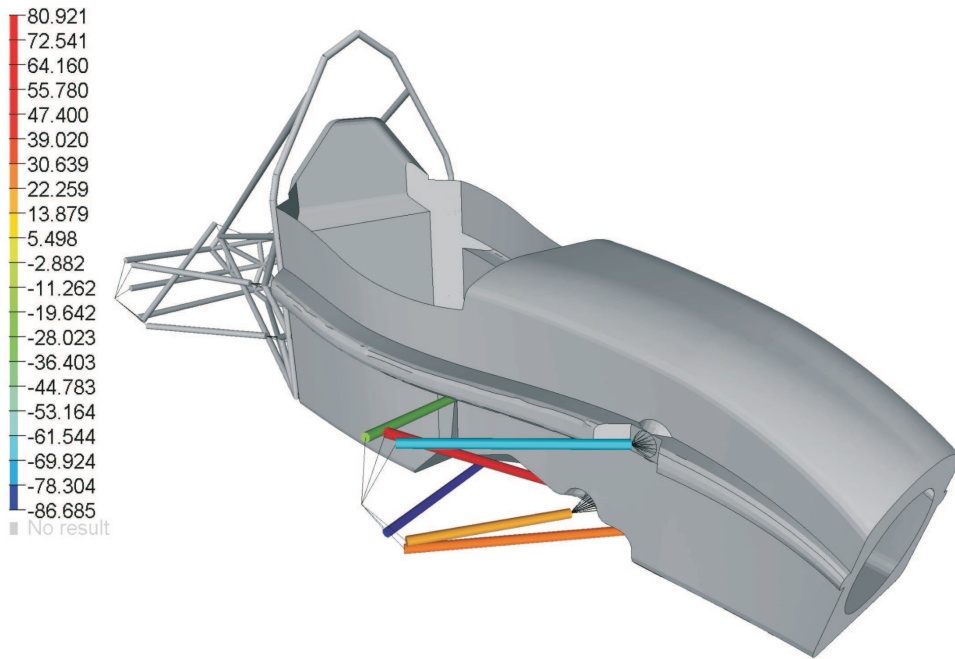


Figure 3.2: The stresses in N/mm² for the front right connection rods for a left corner, while braking and hitting a bump

3.2 Torsional load

To simulate the torsional loads, the maximum vertical wheel load from Table 3 of 4.3 kN is used. A safety factor is applied and the torsional load is modeled as two vertical loads of 10 kN in opposite direction on the front wheel hubs. This load is used to determine the stiffness of the chassis, to identify geometrical inefficiencies and to analyse the rear frame.

3.3 Front impact load

A static analysis of a front impact situation is mandatory. The force that acts upon the front bulkhead of the chassis was calculated in section 2.3 being about 120 kN. This force is evenly distributed over the outer edge of a front bulkhead going straight into the side walls of the chassis structure.

Chapter 4

Overview of used materials

For a closed box structure with a high specific stiffness, relevant criteria for the materials used are, according to Oomen [16]:

- $\frac{E}{\rho}$, the specific modulus in tension or compression
- $\frac{G}{\rho}$, the specific shear modulus
- $\frac{E}{\rho^2}$ or $\frac{E}{\rho^3}$, in bending or buckling where $E \cdot I$ is the relevant parameter

Carbon fiber reinforced plastics are very useful in such structures considering their high specific modulus. Even more so in the form of sandwich panels, to increase the bending stiffness of plates (see Chapter 5). These sandwich laminates are constructed from several plies of CFRP and a core material (Figure 4.1). The fibers are oriented in a certain direction and held together and protected by a resin

The local ply orientation is indicated with respect the laminate main direction \bar{e}_1 or global x-axis (see Figure 3). Typically 0° and 90° plies are used to increase bending stiffness and 45° laminae are used to increase torsional rigidity (see section 4.5).

Most materials used in the chassis cannot be chosen solely based on their properties. The race team has several technical partners and is often reliant on those partners to provide the materials.

4.1 Fiber Reinforced Plastics

Uni-directional prepreg CFRP plies are supplied by a technical partner. These are sheets of carbon fibers pre-impregnated with a resin. Uni-directional or u.d. means that a large percentage of the fibers has the same orientation. These plies allow for higher specific moduli in the main fiber direction compared to for instance $0^\circ/90^\circ$ woven semi-isotropic preps with comparable mass and density. This has to do with the percentage of the total amount of fibers in a certain direction and that in a woven ply, these fiber are not completely stretched to start with (Figure 4.2). Woven plies are however easier in the manufacturing process. The first argument also touches on the most important quality parameter of CFRP's, the

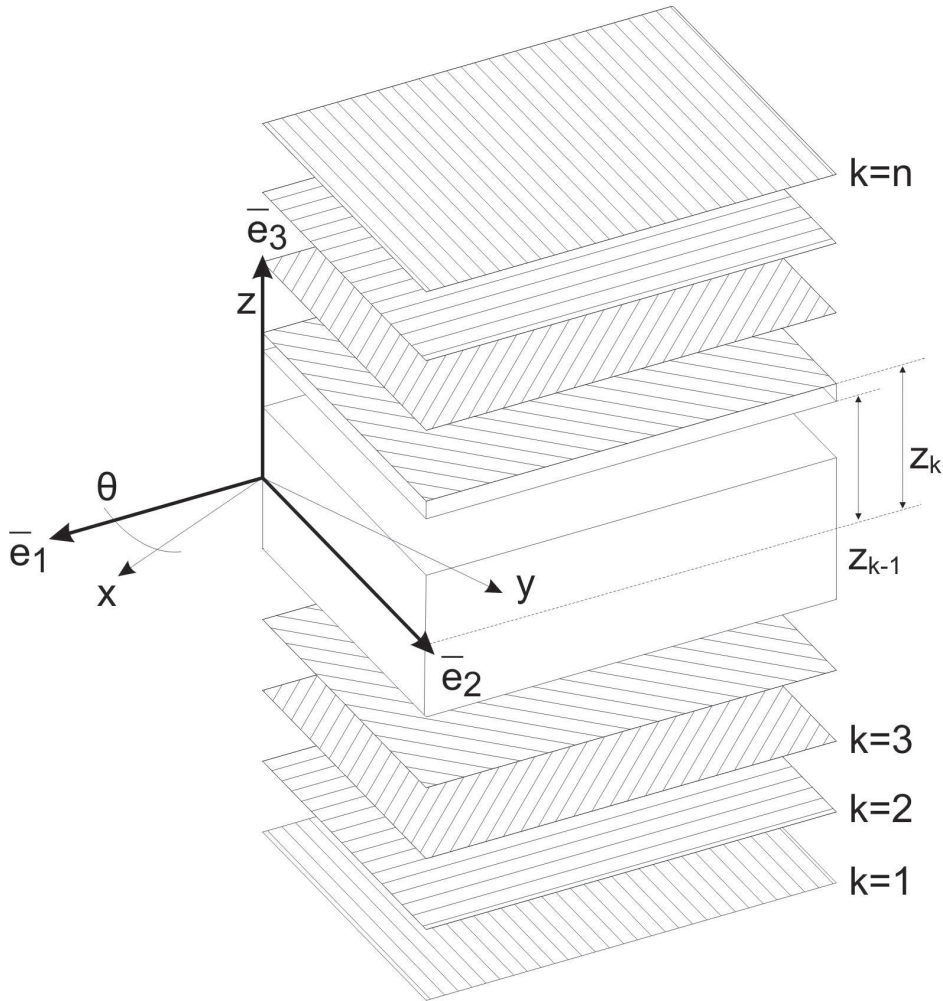


Figure 4.1: A typical laminate using CFRP's and a PVC core

fiber percentage V_f , defined as the total fiber volume divided by the total laminate volume. In practice this must be kept as high as possible.

$$V_f = \frac{\text{fiber volume}}{\text{laminate volume}} \quad (4.1)$$

Because of their specific properties, u.d. prepgs allow for in material engineering by varying ply fiber direction and the number of plies. They has some implications for the design in general:

- The laminate must be carefully constructed to ensure symmetric properties of the sandwich panels with respect to the core
- For a known stress distribution the materials anisotropic character can be used optimally
- The stress distribution can be homogenized by locally strengthening the laminate at the hardpoints

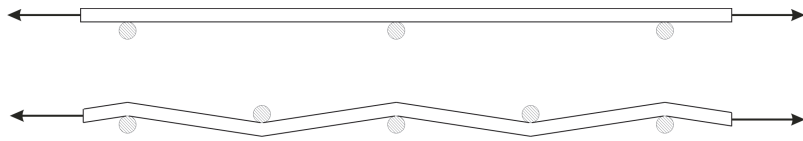


Figure 4.2: u.d. and $0^\circ/90^\circ$ woven prepeg

- By varying the core thickness the structures bending and buckling strength can be increased severely
- The final product quality becomes less sensitive to manufacturing skill due to a predetermined fiber percentage

On the other hand some problems must be taken into consideration:

- The prepgs require high end tooling and production facilities
- Laminate edges can be problematic and must be specifically designed
- De final product quality is highly determined by the manufacturing process
- The used molds must be high temperature and pressure resistant

The required tooling and production facilities are currently available to the team, as is the knowledge to use these facilities. The cheap and abundant labor available in the team can be used to complete the labor intensive manufacturing process. A good alternative for the future is to focus on vacuum injection molding processes. These processes use dry (prewoven) plies and insert the resin by applying a vacuum at one end of the mold and inserting resin in the other. The vacuum sucks the resin through as well as providing a surface finish at the mold side due to atmospheric pressure at the open side. This is a process that requires hardly any high end manufacturing facilities. Also the molds need not to be high pressure and temperature resistant. In the past these techniques were only capable of achieving low fiber percentages, however current technology achieves the same percentages as the use of prepgs. A technical partner has been approached however a interesting cooperation wasn't established.

Alternative fibers to use are E-glass, S-glass, aramid (Kevlar 49) or P.E. fiber. Carbon fibers are however far superior when it comes to specific moduli where aramid is superior when it comes to specific strength. One could consider in future designs to implement aramid fibers in crash sensitive parts of the structure.

Alternative resins are polyester and vynylester. They are outperformed by epoxy however with respect to ultimate strength, bonding properties and temperature resistance [16]. In addition epoxy shows very good fatigue properties and low cure shrinkage in manufacturing [18].

The properties of several fiber materials are shown in Table 4.1. These can only be used as an indication, actual parameters should be obtained by testing. An additional benefit is then that the influence of the manufacturing process is accounted for. In Figure 4.3 trends for the specific stiffness and strength of commonly used structural materials are shown (all fiber materials are u.d. epoxy composites) [18]. The materials available to URE, are in the middle region of the IM Carbon composites.

	Glass [16]	Kevlar 49 [16]	u.d. CFRP ¹	0°/90° CFRP
V_f [-]	0.45	0.60	0.6	0.6
ρ [kg/m ³]	1800	1460	1578	1578
E_1 [N/mm ²]	38600	76000	145000	77500
E_2 [N/mm ²]	8270	5500	9500	77500
G_{12} [N/mm ²]	4100	2300	5800	5800
ν_{12} [-]	0.26	0.34	0.25	0.31
ν_{21} [-]	0.056	0.025	0.016	0.31
X [N/mm ²]	1062	1400	1550	
X' [N/mm ²]	610	235	1250	
Y [N/mm ²]	31	12	70	
Y' [N/mm ²]	118	53	200	
S [N/mm ²]	72	34	90	
t [mm]	0.2	0.2	0.2	0.4

Table 4.1: Mechanical properties of several fiber materials

With:

V_f = fiber percentage

ρ = Material density

E_1 = Elasticity modulus in the fiber direction

E_2 = Elasticity modulus transverse to the fiber direction

G_{12} = In-plane shear modulus

ν_{ij} = poisson's ratio's

X = Longitudinal tensile strength of a u.d. ply

X' = Longitudinal compressive strength of a u.d. ply

Y = Transverse tensile strength of a u.d. ply

Y' = Transverse compressive strength of a u.d. ply

S = Inter- and intra-laminar shear strength of a u.d. ply

t = ply thickness of a u.d. ply

¹The properties for CFRP's are obtained from Futura BV, the teams technical partner on CFRP's products

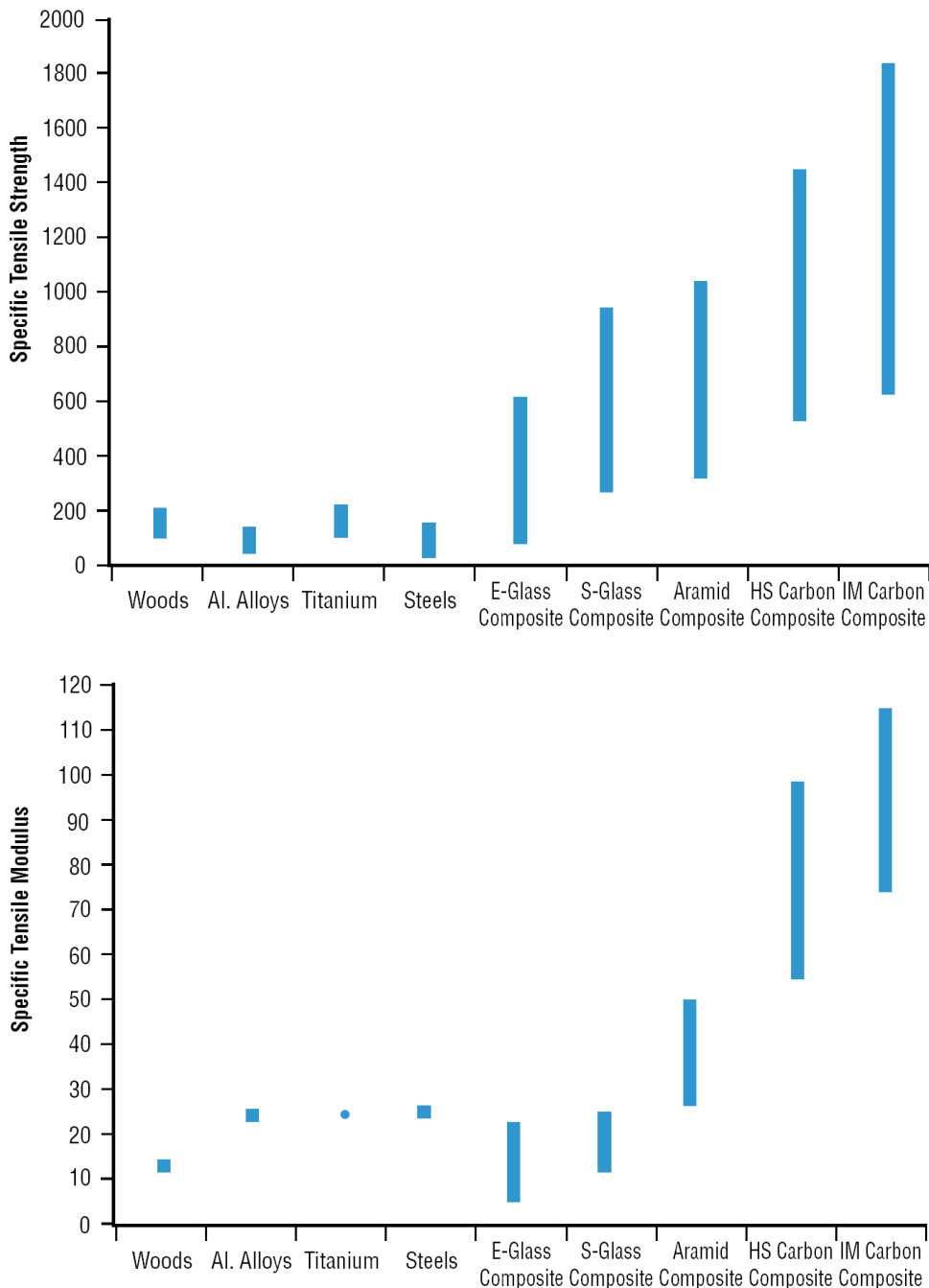


Figure 4.3: Trends for the specific strength $\frac{X}{\rho}$ and modulus $\frac{E_1}{\rho}$ of structural materials and u.d. fiber composites [18]

4.2 Core materials

A selection of Rohacell® core materials are available from one of the teams technical partners. They are PVC foams already widely used in composites sandwich structures. The foams are easily processable, cheap and isotropic, making them easy to model.

Relevant properties of core materials are:

- Specific shear-modulus and strength
- Specific compression-modulus and strength

Alternative core materials are (balsa-)wood and alloy or aramid honeycomb. The honeycomb structures are far superior to foams regarding strength properties. They are however rather expensive and difficult to bond to the laminate faces. It is advisable however to investigate the possibilities of obtaining a technical partner that can provide Nomex® honeycomb. This is an aramid based paper honeycomb structure and its difficulties in production are far outweighed by its specific strength. The honeycomb stiffness properties however appear to be lagging behind compared to the high end Rohacell® foams. The properties of several core materials are shown in Table 4.3. In Figure 4.4 the specific strengths in compression and shear are shown for several core materials.

	Rohacell® 71 IG ²	Rohacell® 110 IG	Rohacell® 200 WF	Aluminum honeycomb [18] ³	Nomex® honeycomb [18]
ρ [kg/m ³]	75	110	205		
E_1 [N/mm ²]	92	160	350		≈ 0.45 [4]
E_3 [N/mm ²]				16-148 ⁴	≈ 120 [4]
G_{12} [N/mm ²]	29	50	150	7-31	2-9
G_{13} [N/mm ²]				14-63	3.7-17
X [N/mm ²]	2.8	3.5	6.8		
X'_1 [N/mm ²]	1.5	3.0	9.0		125-1870
X'_3 [N/mm ²]				4.2	73-620
S_{12} [N/mm ²]	1.3	2.4	5.0	1.48	45-395
S_{13} [N/mm ²]				2.38	85-480

Table 4.2: Mechanical properties of several core materials

²Rohacell® properties are obtained from Evonik Röhm GmbH

³Honeycomb density is strongly dependent on core thickness and cell size

⁴Compressive modulus in local z-direction - i.e. the cell direction for honeycombs

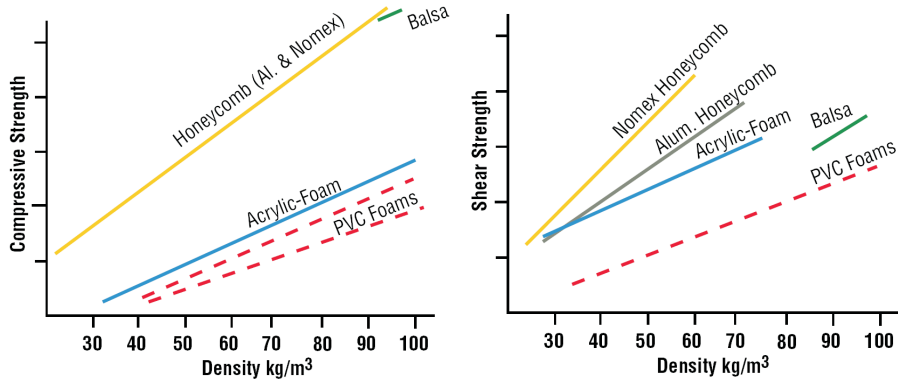


Figure 4.4: Specific compressive and shear strength of core materials [18]

4.3 Core insert materials

At the so called hard points, where transverse forces interface with the monocoque, local strengthening of the core is required to redistribute the concentrated loads. This is achieved by replacing the core locally with stiffeners of a less compliant material (Figure 4.5). It should be able to withstand the compression forces implied by a bolted-on mounting bracket while bending enough to prevent high peak stresses around its circumference [6]. This can be done by choosing the correct material and creating a smooth geometrical boundary between the core materials. A well-known insert material aluminum although conventional plywood as well as end-grain balsa wood show very interesting properties for this purpose [6]. This is more thoroughly explained in sections 4.8 and 4.9.

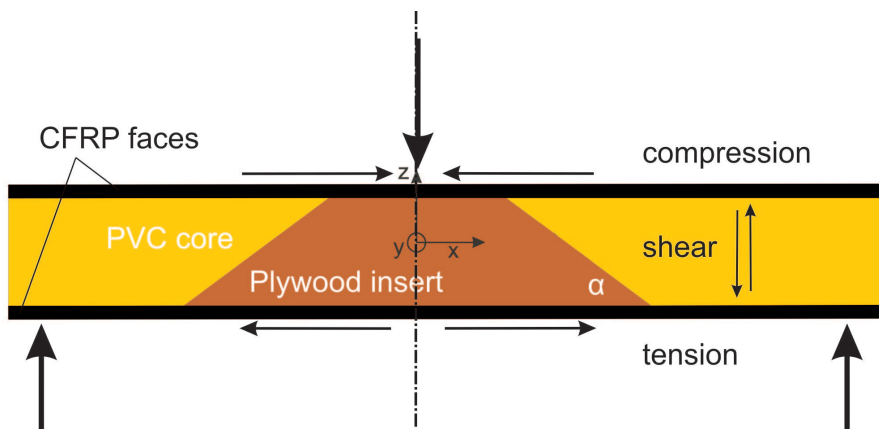


Figure 4.5: Typical transverse loading of a sandwich panel with insert

⁵<http://www.matweb.com> for DIAB ProBalsa® HW

	Aluminum	Birch plywood [5]	end-grain balsa ⁵	Epoxy adhesive [8]
ρ [kg/m ³]	2700	750	221	
E_1 [N/mm ²]	70000	7070	6.8	2500
E_3 [N/mm ²]		1130		
G_{12} [N/mm ²]		530	230	
G_{13} [N/mm ²]		130		
ν_{12} [-]	0.3	0.31		0.3
ν_{13} [-]		0.05		
X [N/mm ²]		31	20.6	50
X' [N/mm ²]			21.9	200
S [N/mm ²]			4.5	45

Table 4.3: Mechanical properties of several core materials

4.4 Tube materials

Colddrawn seamless tube is readily available for the team and it is used for the main and front roll hoops and its bracing. This material has a yield strength of 350 – 700 N/mm². One could use higher end materials such as chrome-moly steel, however the minimum dimensions prevent the application of tubes with a smaller wall thickness, so the benefit in weight savings using stronger steel cannot be obtained. Regarding the rear frame however the tube material can be freely chosen as well as its dimensions. For manufacturing convenience however the same material is used and only the geometry is varied to cope with the applied loads. Hereby the outer diameter of the rear frame tubes is kept the same as the roll hoop, again for manufacturing ease, so the only variable becomes the wall thickness.

4.5 Global laminate stiffness

To calculate the chassis stiffness and global first ply failure Altair Hyperworks® uses the classical laminate theory to transform local ply properties to global laminate properties. The global and local strain directions and ply angles were already defined in Figure 4.1. The following macromechanic assumptions are made for laminate calculation [13]:

- Uniform linear strain and stress distribution
- Plane stress conditions
- Each ply is quasi-homogeneous and orthotropic. This means the material properties are symmetric with respect to the two perpendicular planes through the main strain directions x and y.
- Flat laminate sections remain flat in both tension and compression. This is due to the plane stress assumption. Combined with the plane stress condition it reduces the number of independent material parameters to 4 (E_x , E_y , ν_{xy} and G_{xy})
- The bonding between the plies is assumed to be homogeneous

Consider plane stress conditions (out-of-plane stress $\sigma_z = \text{perpendicular shear stress } \tau_{xz} = \tau_{yz} = 0$) of an orthotropic u.d. ply of CFRP. For a ply k with its midplane at a distance z_k with respect to the local ply reference plane through \bar{e}_1 and \bar{e}_2 with $z = 0$, the compliance constitutive relation comes down to [11][13]:

$$\begin{aligned}\bar{\sigma} &= \bar{Q} \cdot \bar{\varepsilon} \\ \begin{bmatrix} \sigma_1 \\ \sigma_2 \\ \tau_6 \end{bmatrix} &= \begin{bmatrix} Q_{11} & Q_{12} & 0 \\ Q_{12} & Q_{22} & 0 \\ 0 & 0 & Q_{66} \end{bmatrix} \begin{bmatrix} \varepsilon_1 \\ \varepsilon_2 \\ \gamma_6 \end{bmatrix} \\ \begin{bmatrix} \sigma_1 \\ \sigma_2 \\ \tau_6 \end{bmatrix} &= \begin{bmatrix} \frac{E_1}{1-\nu_{12}\nu_{21}} & \frac{\nu_{21}E_1}{1-\nu_{12}\nu_{21}} & 0 \\ \frac{\nu_{12}E_2}{1-\nu_{12}\nu_{21}} & \frac{E_2}{1-\nu_{12}\nu_{21}} & 0 \\ 0 & 0 & G_{12} \end{bmatrix} \begin{bmatrix} \varepsilon_1 \\ \varepsilon_2 \\ \gamma_6 \end{bmatrix}\end{aligned}\quad (4.2)$$

With σ_1 and σ_2 the local in-plane normal stresses, τ_6 the in-plane shear stress and Q_{ij} the corresponding stiffness with respect to the in-plane normal strains ε_1 and ε_2 and the in-plane shear strain γ . E is the modulus of elasticity and ν poisson's ratio. Transformation to the global laminate directions \bar{e}_x and \bar{e}_y gives:

$$\begin{aligned}\begin{bmatrix} \sigma_x \\ \sigma_y \\ \tau_s \end{bmatrix} &= \bar{Q}' \begin{bmatrix} \varepsilon_x \\ \varepsilon_y \\ \gamma_s \end{bmatrix} \\ \begin{bmatrix} \sigma_x \\ \sigma_y \\ \tau_s \end{bmatrix} &= \begin{bmatrix} Q_{xx} & Q_{xy} & Q_{xs} \\ Q_{xy} & Q_{yy} & Q_{ys} \\ Q_{xs} & Q_{ys} & Q_{ss} \end{bmatrix} \begin{bmatrix} \sigma_x \\ \sigma_y \\ \tau_s \end{bmatrix}\end{aligned}$$

Because of the assumption of a flat laminate remaining flat we can write the ply strains in global coordinates with respect to the laminate reference plane ($z=0$) as:

$$\begin{bmatrix} \varepsilon_x \\ \varepsilon_y \\ \gamma_s \end{bmatrix} = \begin{bmatrix} \varepsilon_x^0 \\ \varepsilon_y^0 \\ \gamma_s^0 \end{bmatrix} + z \begin{bmatrix} \kappa_x \\ \kappa_y \\ \kappa_s \end{bmatrix} \quad (4.3)$$

With ε_x^0 , ε_y^0 and γ_s^0 the strains of ply k projected on the reference plane, κ_x , κ_y , κ_s the curvatures of the ply and z the distance of the ply midplane to the laminate reference plane. Now using the strains from equation 4.3 and looking at Figure 4.6 we can write the laminate stiffness matrix as:

$$\begin{bmatrix} N_x \\ N_y \\ N_s \\ M_x \\ M_y \\ M_s \end{bmatrix} = \begin{bmatrix} A_{xx} & A_{xy} & A_{xs} & B_{xx} & B_{xy} & B_{xs} \\ A_{xy} & A_{yy} & A_{ys} & B_{xy} & B_{yy} & B_{ys} \\ A_{xs} & A_{ys} & A_{ss} & B_{xs} & B_{ys} & B_{ss} \\ B_{xx} & B_{xy} & B_{xs} & D_{xx} & D_{xy} & D_{xs} \\ B_{xy} & B_{yy} & B_{ys} & D_{xy} & D_{yy} & D_{ys} \\ B_{xs} & B_{ys} & B_{ss} & D_{xs} & D_{ys} & D_{ss} \end{bmatrix} \begin{bmatrix} \varepsilon_x^0 \\ \varepsilon_y^0 \\ \gamma_s^0 \\ \kappa_x \\ \kappa_y \\ \kappa_s \end{bmatrix} \quad (4.4)$$

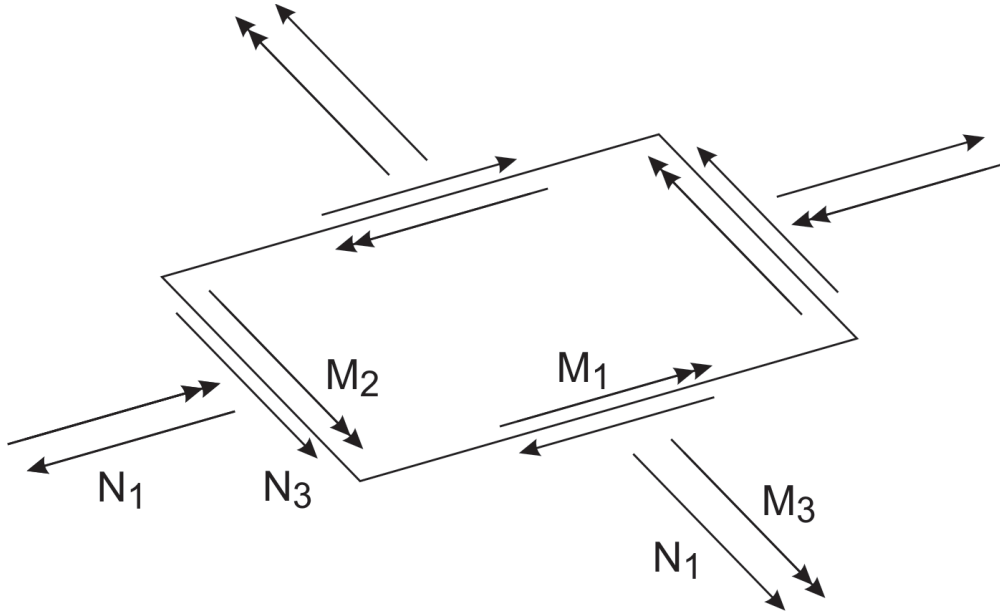


Figure 4.6: Loads on a piece of sandwich

This matrix is crucial as it allows the engineer to actively tune the contribution of each ply to the global laminate behavior under different loading conditions. It is constructed by adding the contributions of all plies. In this compiled stiffness matrix the in-plane stiffness is represented by \bar{A} , of which the components can be written in terms of the distance of each ply to the reference plane $z_k - z_{k-1}$:

$$A_{ij} = \sum_{k=1}^n (Q'_{ij})_k \cdot (z_k - z_{k-1}) \quad (4.5)$$

The coupling matrix \bar{B} represents bending of the laminate by in-plane forces and in-plane strains caused by out-of-plane moments and is governed by the square of z :

$$B_{ij} = \frac{1}{2} \sum_{k=1}^n (Q'_{ij})_k \cdot (z_k^2 - z_{k-1}^2) \quad (4.6)$$

The bending stiffness of the laminate is represented by matrix \bar{D} which is determined by the third power of z :

$$D_{ij} = \frac{1}{3} \sum_{k=1}^n (Q'_{ij})_k \cdot (z_k^3 - z_{k-1}^3) \quad (4.7)$$

The exact contribution of the fibers and resin materials to the laminate stiffness considering ply angles and fiber percentage is investigated more thoroughly in [11]. In this project Altair Hyperworks® is used to calculate the equivalent stiffness matrices \bar{A} , \bar{B} and \bar{D} . Hereby the ply thickness and angle can be varied, as well as the core thickness. It becomes clear immediately that the bending stiffness is heavily dependant on the core thickness (increase in z) while the in-plane stiffness can be tuned by varying the u.d. ply angles. The laminate should be symmetric with respect to its midline to prevent unwanted bending due to in-plane loads and in-plane stresses due to applied moments. In addition Altair Hyperworks® calculates the equivalent material parameters with respect to the global laminate directions to quickly check the effect of changes in the lay-up. A typical laminate build-up in Hyperworks® is shown in Figure 4.7.

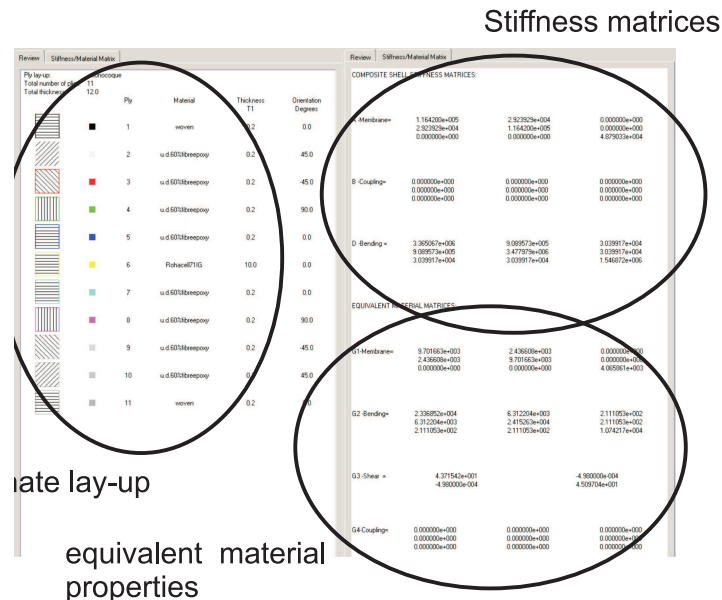


Figure 4.7: A typical lay-up in Altair Hyperworks® (left) with equivalent material matrices (right)

4.6 Global ply failure

Altair Hyperworks® is also used to evaluate the stresses per ply. The global stresses from section 4.5 are calculated back to the local ply directions to check whether maximum stresses are exceeded. For this purpose several ply failure criteria are used:

1. Tsai-Hill criterium:

A criterium based on the deformation energy and comparable to the Von Mises criterium for isotropic materials:

$$\frac{\sigma_1^2}{X^2} - \frac{\sigma_1\sigma_2}{X^2} + \frac{\sigma_2^2}{Y^2} + \frac{\tau_6^2}{S^2} \leq 1 \quad (4.8)$$

2. Hoffman criterium:

The Tsai-Hill criterium however doesn't account for the differences in tensile and compressive strengths of composites. Hoffman implemented this characteristic and wrote for plane stress conditions:

$$\frac{\sigma_1^2 - \sigma_1\sigma_2}{XX'} + \frac{\sigma_2^2}{YY'} + \frac{X' - X}{XX'}\sigma_1 + \frac{Y' - Y}{YY'}\sigma_2 + \frac{\tau_6^2}{S^2} \leq 1 \quad (4.9)$$

With:

X = Longitudinal tensile strength of a u.d. ply

X' = Longitudinal compressive strength of a u.d. ply

Y = Transverse tensile strength of a u.d. ply

Y' = Transverse compressive strength of a u.d. ply

S = Inter- and intra-laminar shear strength of a u.d. ply

The Hoffman criterium is used and can be easily extracted from analyses in Altair Hyperworks®. Global ply failure typically emerges around discontinuities of the fibers - i.e. around bolt holes, on sharp edges or corners and especially at open fiber ends. They should be avoided where possible. True failure is difficult to analyze because especially around such discontinuities the planes stress assumption doesn't hold. Global ply failure analysis can thus be used as a tool to identify local failure hotspots in the design. If these are caused by avoidable geometrical discontinuities, they are called geometrical inefficiencies, and they should be redesigned. In section 4.8 a more thorough analysis of local laminate behavior is presented.

4.7 Laminate design consideration

From the analysis above and general structural considerations a number of rules of thumb hold for structures built from multi-layer and multi-directional laminates:

- The bending coupling terms B_{ij} are responsible for laminate warpage during curing cool down and thermal loading. These terms should be kept zero by building the laminate lay-up symmetrical with respect to its central reference plane.
- Shear coupling terms A_{xs} and A_{ys} cause in-plane shear deformations under in-plane normal loading. These terms should be kept small by keeping the lay-up balanced and cross-ply. A balanced lay-up means semi-isotropic equivalent properties. A cross-ply lay up is for instance a $0^\circ/90^\circ/90^\circ/0^\circ$ laminate
- The torsion coupling terms D_{xs} and D_{ys} are responsible for twisting deformation under cylindrical load and may cause severe interlaminar stresses in bending. Building the laminate anti-symmetric or cross-ply reduces these terms to zero. The only lay-up that produces all three coupling terms zero is cross-ply symmetric - i.e. $0^\circ/90^\circ/90^\circ/0^\circ$. Symmetric and balanced lay-ups can be created with $B_{ij} = 0$ and $A_{is} = 0$ but usually $D_{is} \neq 0$.
- The difference in orientation between subsequent plies must be kept as small as possible, this will reduce the torsional coupling terms D_{is}
- Avoid laying plies with the same orientation on top of one another, this will reduce the torsional coupling terms D_{is}
- Avoid sharp corners and open fiber ends at loaded edges such as bolt holes

4.8 Local ply failure

At the hardpoints, where loads are entering the chassis perpendicular to the plane, the plane stress assumption is rendered obsolete. Therefor in section 8.5 a 3D analysis of a circular insert is done to evaluate the local stress effects around such an insert. According to Bozhevolnaya *et al* [7] these local effects manifest themselves by significant increases in bending stresses in the vicinity of material discontinuities that come with the use of core inserts. These increased bending stresses are displayed as increases in normal stresses in the sandwich faces and transverse normal (or peel) and shear stresses in the core. The height of the occurring stress peaks around core inserts is determined by two parameters [6]:

$$g = \sqrt{\frac{G_{c1}}{G_{c2}}} \text{ and } \mu = \sqrt{k_v \frac{G_{c1}h_c(h_c + h_f)^2}{E_f h_f^3}} \quad (4.10)$$

With: G_{c1} and G_{c2} the shear moduli of the PVC foam and the insert, respectively, E_f and ν_f the equivalent elastic modulus and poisson ratio of the sandwich faces - i.e. the equivalent parameters of a stacked number of u.d. plies. h_c and h_f are the core and face thickness (see Figure 4.8) and $k_v = (1 - 2\nu_f)/4(1 - \nu_f)$. $N(x)$, $M(x)$

and $Q(x)$ are the global resultants that, according to classical laminate theory are divided over the sandwich parts. The normal force $N(x)$ and bending moment $M(x)$ are carried by the sandwich faces while the shear resultant $Q(x)$ is absorbed by the core.

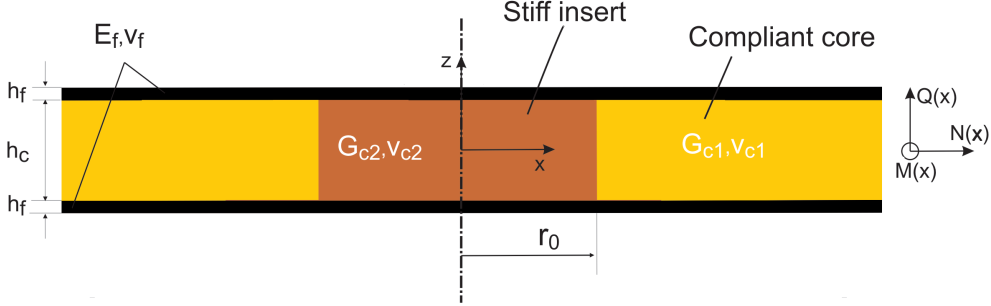


Figure 4.8: A circular non-tapered insert in a sandwich panel

The three main resulting locally induced stresses on the insert/core boundary are: an in-plane bending stress in the faces σ_f , a shear stress in the core $\tau_c = \tau_{zx}$ and a transverse normal/peeling stress in the core $\sigma_c = \sigma_{zz}$ at the upper a lower face/core interfaces. It has been shown that for non-tapered inserts the global shear stress resultant across a core junction $Q(x = 0) = Q_0$ determines the local stress peaks. Assumed for now is the shear stress over the core junction to be constant:

$$\tau_0 = \frac{Q_0}{h_f + h_c} \quad (4.11)$$

The local stress peaks are expressed as a function of this constant shear stress τ_0 [6]:

$$\sigma_f = \tau_0 F_1(g, \mu, x) \frac{h_c(h_c + h_f)}{h_f^2}$$

$$\tau_c = \tau_{zx} = \tau_0 F_2(g, \mu, x) \quad (4.12)$$

$$\sigma_c = \sigma_{zz} = \pm \tau_0 F_3(g, \mu, x)$$

Herein the factor functions F_1 , F_2 and F_3 depend on the two parameters of Eq.(4.10) and dominate the behavior of local stresses over the insert/core boundary. The length over which these local effects disturb the global stress balance is expressed dimensionless and shown in Figure 4.9 for two scenario's. A very stiff, steel, insert in a compliant core (left) and a more compliant, plywood, insert in the same core (right). Important is to see that not the height of the peak is of importance but the localization of discontinuities in the factor functions. A plywood insert leads logically to lower material discontinuities and much smoother curves in Figure 4.9. The characteristic length from the insert/core boundary after which the local stress effects stop being of importance is h_c , so it is advisable in designing inserts to stay away from geometrical discontinuities a distance of approximately the core thickness.

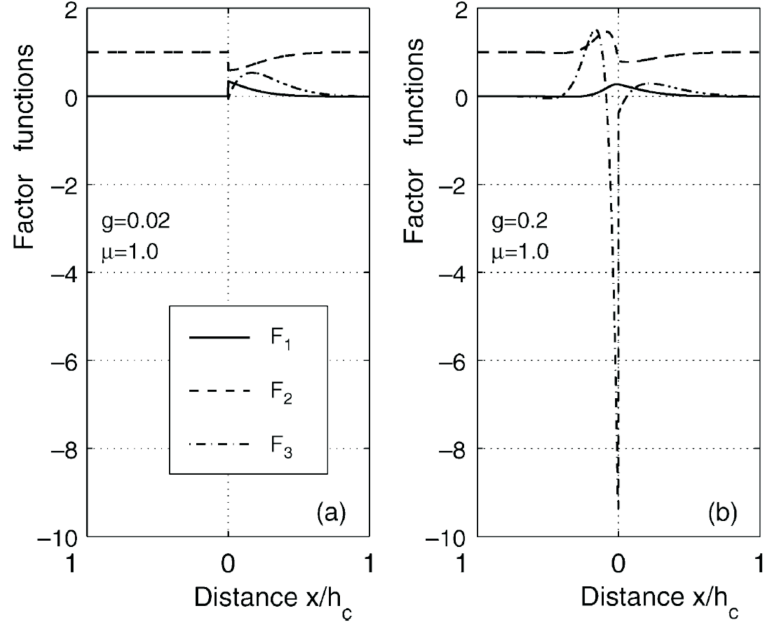


Figure 4.9: Discontinuity of the form factors whose shape determines local stress effects around an insert/core boundary: (left) a steel insert in a compliant core (right) a plywood insert in the same core [6]

Furthermore the functions from Eq. (4.13) only hold for the following conditions:

$$h_f^2 \ll h_c^2, E_f h_f \gg E_c h_c, r_0 \gg h_c \quad (4.13)$$

With r_0 being the radius of the insert. In order to estimate the local effects on the insert/core boundary the factor functions F_1 , F_2 and F_3 can be looked up in Figures 4.10a-d and implemented in Eq. (4.13). These form factors are derived in detail in [6].

This analytic model has been compared extensively to FEA results and good similarities have been found for the all three locally induced stress peaks σ_f , τ_c and σ_c [6]. The model used in this reference is extended and used to analyze the particular application discussed in this report and presented in section 8.5.

In the theory described in this section an important factor is missing though. In the analysis of Bozhevolnaya *et al* the load is applied as a pure shear force Q_0 at the centerline the insert. In reality the force is inserted into the sandwich by a mounting bracket that is glued to the top face of the sandwich. The edges of this mounting bracket form another material discontinuity that cause localization of stresses due a step in the section area perpendicular to the plane in Figure 4.11. The peaks in the stresses due to this mounting bracket are actually much higher then the peaks due to the insert/core boundary. In section 8.5 the occurring local stresses are analyzed and different measures to reduce the stress localization are described in the following section.

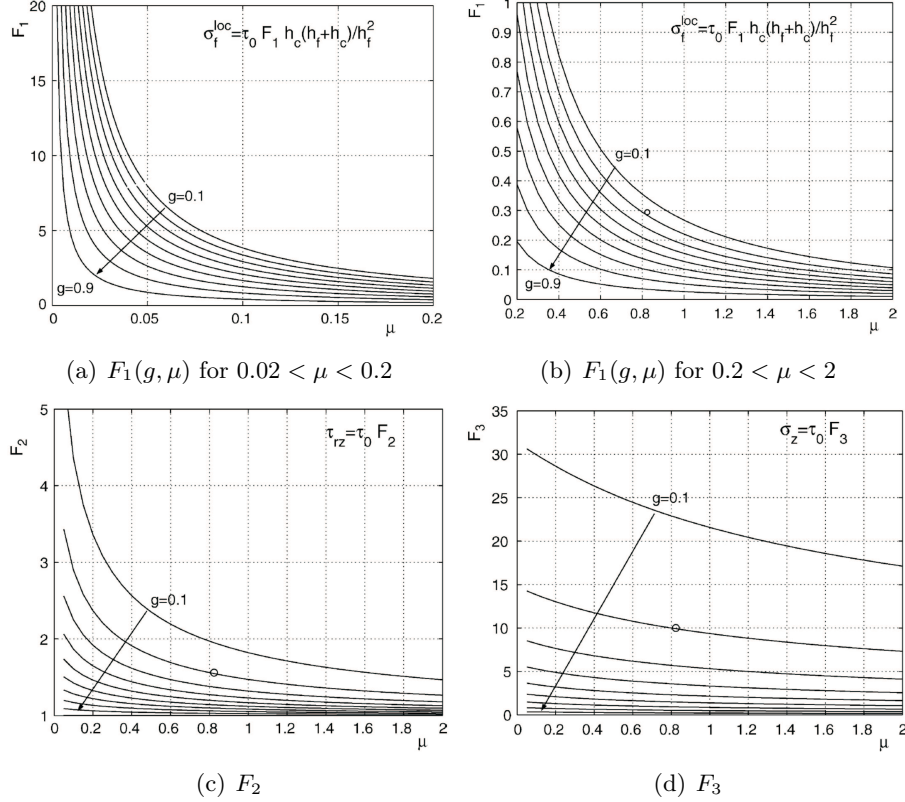


Figure 4.10: Charts of form factors for calculation of local peak stresses [6]

4.9 Insert design consideration

To reduce the local effects around insert/core boundaries and at the mounting bracket edges a number of measures can be taken. The first is to reinforce the CFRP-plies externally to allow them to absorb the induced local stress peaks (Figure 4.11). Perhaps not surprisingly this *local strengthening* reduces all three of the local stress effects, and not just the normal in-plane stress in the sandwich faces σ_f . However it creates another material discontinuity around its edge and to prevent local effect influencing each other the radius of the ply strengthening should be about h_c away from other discontinuities.

The second is to reduce the material discontinuities across core junctions - i.e. reduce g by choosing a material that has G_{c2} closer to G_{c1} . To still provide enough stiffness in the hardpoint one might want to add an additional ring of insert material around the insert that has properties in between those of the insert and the compliant core. A so called *core patch* (Figure 4.11).

The third is to decrease the material discontinuity geometrically by tapering the insert as shown in Figure 4.11 and secondly by making sure the applied force on the outer face is introduced into the sandwich panel gradually by tapering the mounting bracket and making sure the force approaches under an angle (a practi-

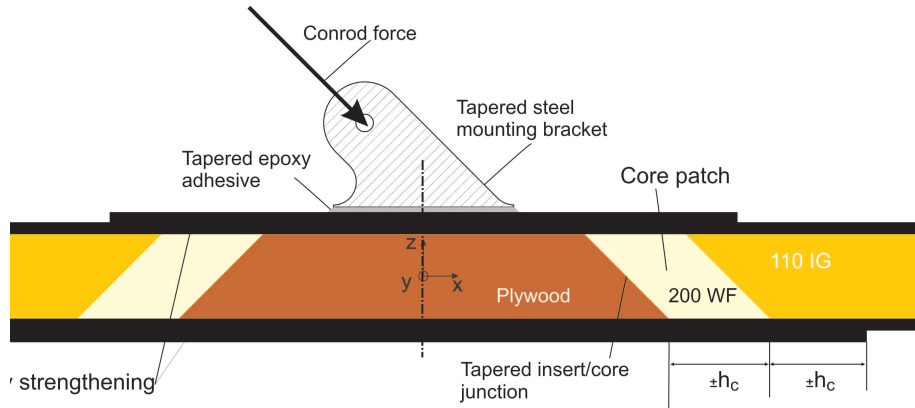


Figure 4.11: Reducing the local stresses around hardpoints

cal value is 45°). The other measures have been investigated by Bozhevolnaya *et al* [7][6][5] and the results are shown in Figure 4.12.

The analytic model from section 4.8 clearly shows that the shear moduli of adjacent inserts and cores play a major role in the occurrence of local stress peaks. However the main goal of inserts is to locally strengthen the sandwich to distribute transverse loads. Thus while a small G_{c2} for the insert is desirable at the same time a large transverse stiffness is of interest. This implies the use anisotropic materials would be very interesting for inserts with a high transverse elastic modulus E_3 and a small transverse shear modulus G_{13} . This is the case for plywood and especially for end-grain Balsa which shows an extremely large ratio between transverse elastic and shear moduli:

$$\text{Birch-plywood: } E_c/G_c = 1130 \text{ N/mm}^2 / 130 \text{ N/mm}^2 = 8.7$$

$$\text{DIAB ProBalsa}^\circledR \text{ HW: } E_c/G_c = 6840 \text{ N/mm}^2 / 240 \text{ N/mm}^2 = 28.5$$

It is therefore advisable to investigate the use of DIAB ProBalsa[®] HW to create tapered inserts that are reinforced by additional plies of CFRP.

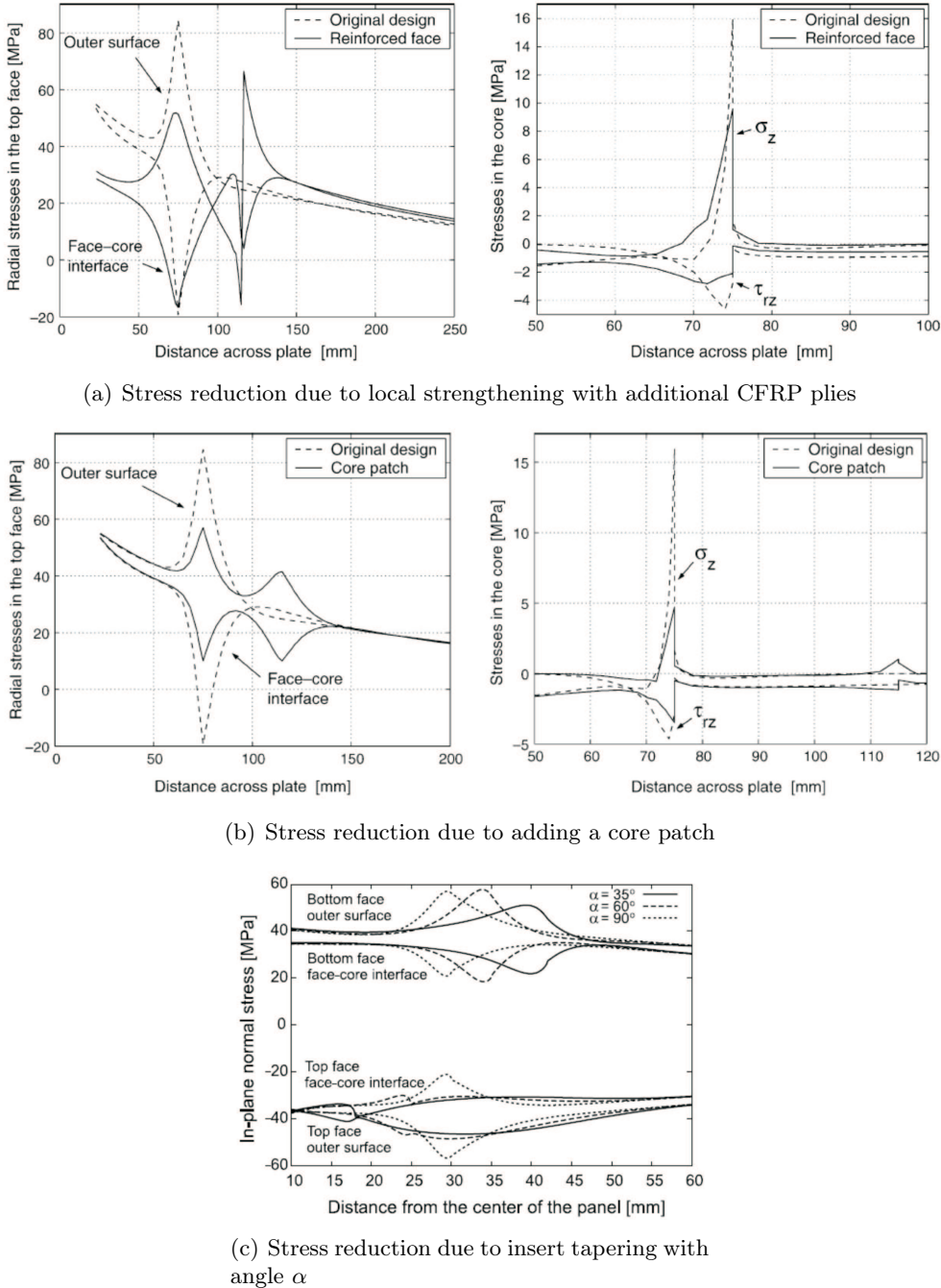


Figure 4.12: Effects of several measures to reduce local stresses around inserts
[6][5]

Chapter 5

General structural considerations

As mentioned in Chapter 2 the designed monocoque should be stiff in torsion as well as having high strength in tension, bending and buckling. Firstly a simplified approach to achieving torsional stiffness is introduced. Secondly this is combined with manufacturing simplicity and the rules that apply to the structural cockpit. Then is analyzed where equivalency with a steel tubular frame is required so the material can be engineered to do so.

5.1 Torsional stiffness

For a closed box structure very high torsional stiffness is achievable with a very small wall thickness, provided that section cuts perpendicular to the torsion axis remain the same shape. In the of the UREo5 however the cockpit opening is large compared to the overall structure. The minimum cockpit opening is mandatory (see Appendix B). This means that it becomes an open box structure. The closed edges in part I of the cockpit are still loaded with shear stresses while the open edges in part II are subject to bending stresses and want to form an 'S-shape'. A simplified overview of the cockpit is shown in Figure 5.1. It is illustrated how the closed edges are subject to shear stresses while the open edges experience bending stresses.

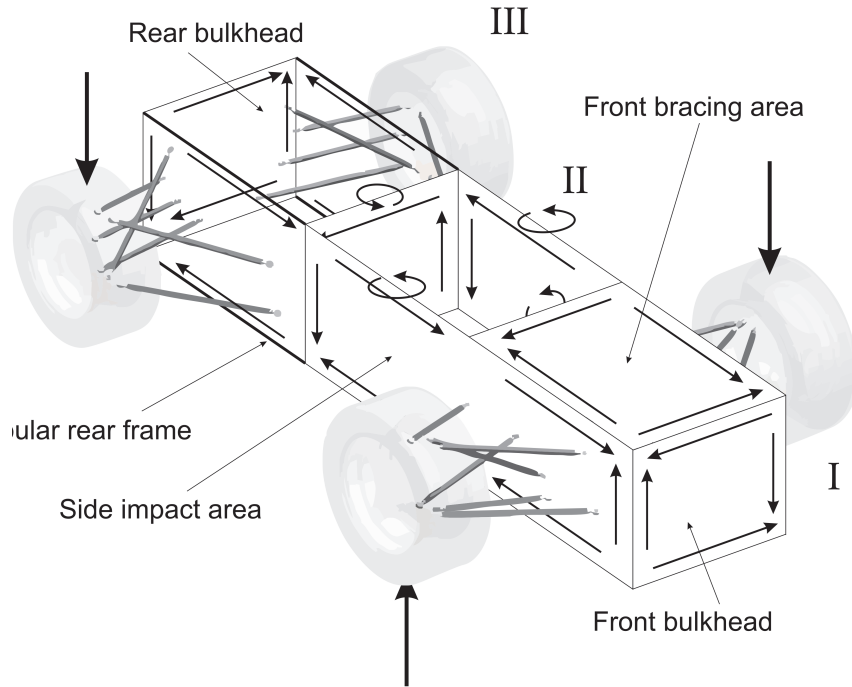


Figure 5.1: A simplified overview of the chassis in three parts: I, a closed profile, II, an open profile and III, a tubular space frame

In Figure 5.2 section cuts are shown for a closed and an open profile. The torsional stiffness for these profiles is $k = GI/l$. For similar material and length l the stiffness is determined by the *second moment of area* I .

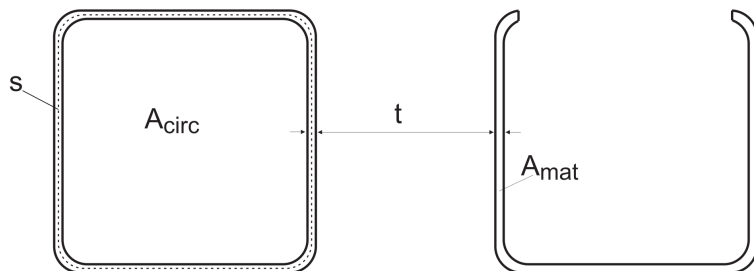


Figure 5.2: Torsion stiffness in a closed profile depends on the enclosed volume while for an open profile the thickness of the material is dominant

For the second moment of area of a closed profile, I_c , and an open profile, I_o , we can write [14]:

$$I_c = \frac{4A_{circ}t}{O} \quad (5.1)$$

$$I_o = \frac{A_{mat}t^2}{3}$$

With A_{circ} the surface enclosed by the perimeter O over the center line s , t is the thickness and A_{mat} the surface of the section material. For a closed profile the material is used about three times as effective in resisting torsion. Looking at the weakest link the open section must be made stiffer in torsion. Hereto the wall thickness can be increased as well as the amount of material in the section.

Very important is the resistance of the plates that form the profile to shear stresses. As can be seen from Figure 5.1 the main load on the panels is shear stress. The fibers must in this case be placed under an angle of 45° and -45° to provide maximum equivalent panel shear stiffness. The panels that experience bending moments should have fibers in the 0° and 90° direction for optimal bending stiffness

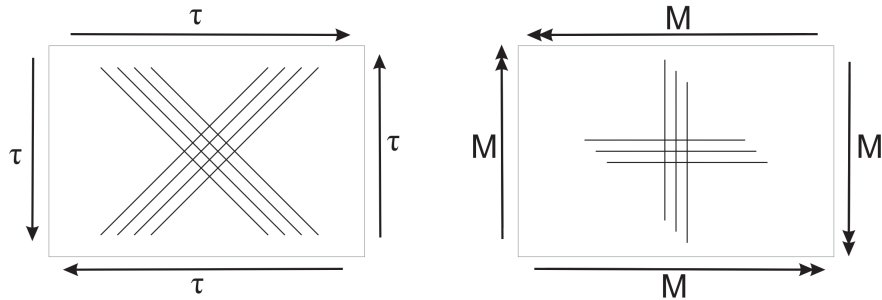


Figure 5.3: Fiber direction for large shear (left) and bending (right) stiffness in sandwich panels

To keep the section cuts in Figure 5.2 in the same shape under a torsional load perpendicular to the plane, one could make a significant stiffness increase by adding bulkheads on certain points in the structure, preferably where loads enter the chassis. They would keep the section of the open box the same shape thus increasing the resistance to torsional deflection [14]. The placement of bulkheads however means an increase in the number of components and manufacturing complexity in general. If possible this should be prevented.

Furthermore the load is not pure torsion. It must be taken care of that where the loads enter the structure, plate is placed in the proper direction - i.e. the loads are applied in-plane instead of perpendicular to the plane.

5.2 Bending stiffness

If one needs the open box structure in Figure 5.1 to be stiff in torsion the open part should be focussed on. Hereby the bending stiffness of the open edges is of great importance. As mentioned in Chapter 4 the bending stiffness of a plate depends on EI . A number of possibilities exist to increase the I of a plate:

- Used materials with a high specific stiffness $\frac{E}{\rho}$, $\frac{E}{\rho^2}$ and $\frac{E}{\rho^3}$
- Fold the open edges perpendicular to the plane
- Increase EI by applying ribs over the surface of a plate or an open edge
- Increase EI by making the plate a 3D profile
- Increase EI by applying a sandwich construction

As mentioned in Chapter 4 high specific stiffness materials in a sandwich structure are taken as a starting point. Furthermore, besides increasing I around the open edges, another issue is that one must prevent open ply ends because here delamination typically initiates. In Figure 5.4 is shown how open ply ends can be prevented while increasing the second moment of area I . Looking back at Eq.(5.2) one see right away that an increase in I of the open edge also increase A_{mat} and a local increase in bending stiffness relates to a global increase in torsional stiffness!

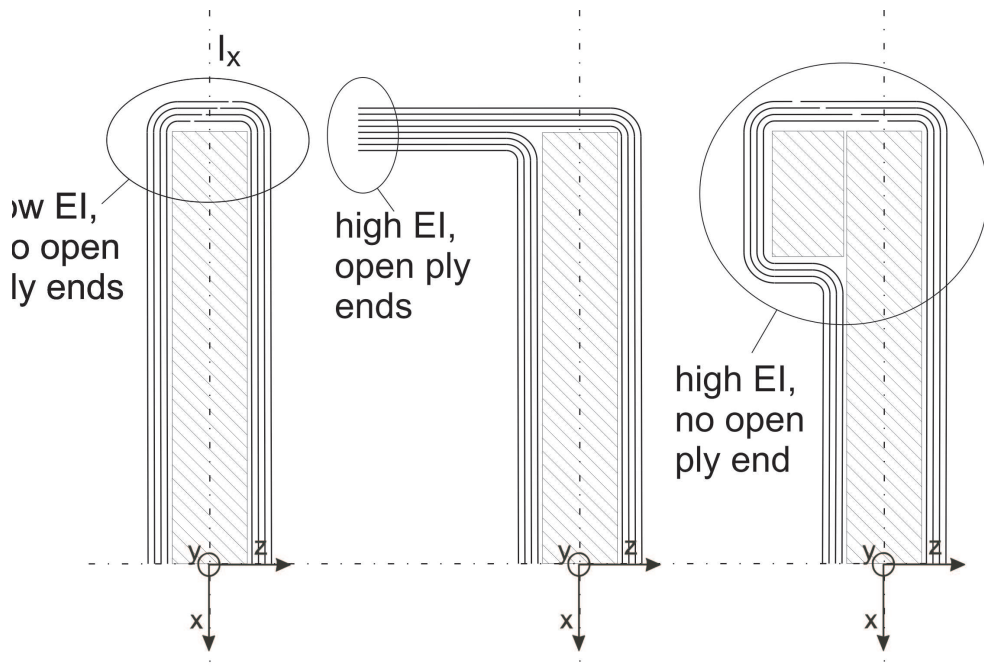


Figure 5.4: Prevent open ply edges (left), increase edge bending stiffness (center) and combining these measures (right)

The same measures are taken for the side impact area and front bracing area where high buckling strength is required. The buckling strength, as well as the bending stiffness for plates depends $E \cdot I$. These two areas can be made strong in buckling mainly by increasing the thickness of the sandwich panels and creating 3D profiles. This is illustrated in sections 8.7 and 8.8. A few possibilities are shown in Figure 5.5. The first option leaves open ply ends, the second one requires an additional production step to apply the stiffener while option three can be manufactured in a single mold.

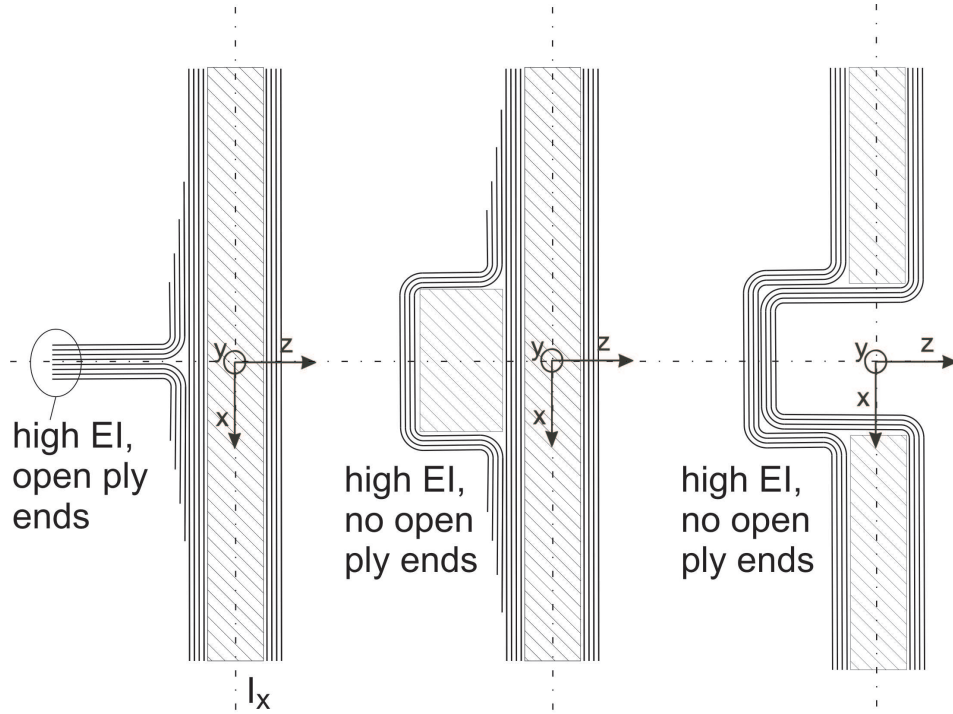


Figure 5.5: Increasing the buckling strength of sandwich plates

5.3 Multi-Shell Assembly Approach

Most options discussed in the previous sections make the monocoque far more complex. When implemented in the chassis to increase the total torsional stiffness, stiffen all the chassis load points and make the side impact and front bracing areas stronger in buckling the chassis becomes very difficult to manufacture.

Weidner *et al* came up with a solution however for implementing complex structural shapes in a simple four part assembly monocoque [10]. They approach the design of a monocoque structure as that of a pressure vessel using two inner shells, that in this case form the two sides of the monocoque, and two outer shells that are used to complete the chassis. By clever implementation of this technique all structural demands can be integrated into only four relatively simple molds.

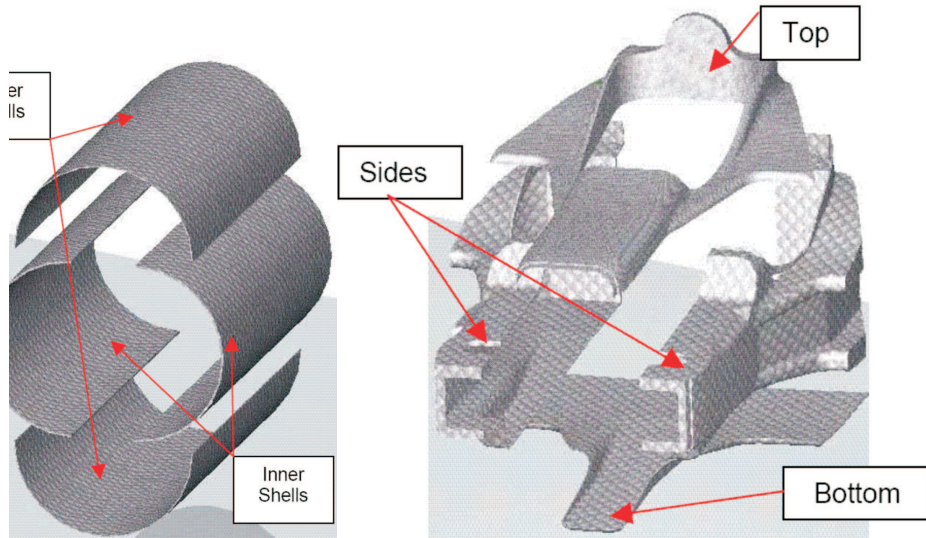


Figure 5.6: The multi-shell Assembly Approach by Weidner *et al* [10]

5.4 Tubular rear frame

In Figure 5.1 the tubular rear frame is shown as part III. To make this frame stiff in torsion triangulation must be applied. A very simple solution is implemented requiring a minimal number of tubes. Three simple 'V-shapes' are combined fixating the rear bulkhead to the monocoque structure. The goal hereby is making the inner angle of the 'V' as large as possible while looking at packaging criteria. This angle must be large to make sure that the used tubing is loaded in tension and compression rather than bending.

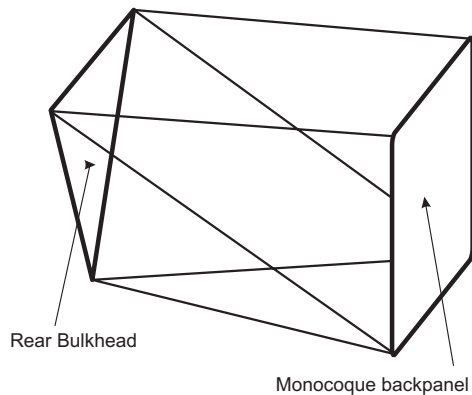


Figure 5.7: A simple though very stiff tubular rear frame

Chapter 6

Ergonomics

One of the most important factors in the Formula Student competition, and in any race competition, is the driver. He or she must be comfortable at all times and able to easily reach all controls. The ergonomics have been investigated using a mock-up to find a good compromise between performance and comfort (see Figure 6.3). The available drivers have been fitted in as well as the 95th percentile male template and all the variables have been determined and implemented in the design.

The variables used in looking for a good seating position of the driver are the following:

- The vertical and horizontal position of the steering wheel
- The horizontal position and angle of the seat with respect to the horizontal
- The horizontal and vertical position of the pedal assembly
- The height and horizontal position of the dashboard and front roll hoop

The goals of this study were:

- Reclined seat back angle with respect to the horizontal: lower the overall center of gravity without compromising the driver's comfort
- Create a seat thigh angle, to prevent the driver from shoving into his or her restraint harness when braking (the restraint harness is mounted in between the driver's legs)
- Steering wheel location in such a way that:
 - the driver can turn the steering wheel without hitting his or her legs
 - the driver can operate the pedals without hitting the steering wheel with his or her legs
- Dashboard/front roll hoop such that:
 - the steering wheel complies to the FSAE rules (see Figure 6.2)
 - the driver can see ahead of the car and especially ahead of the front wheels
- Dash/floor and dash/seat clearance sufficient to pass the cockpit template test (see Appendix B)

- Position of the pedal assembly so that all drivers can easily reach them
- Determine the dashboard/front roll hoop height in such a way that the helmet clearance rule for a 95th percentile male is met (see Figure 6.1)

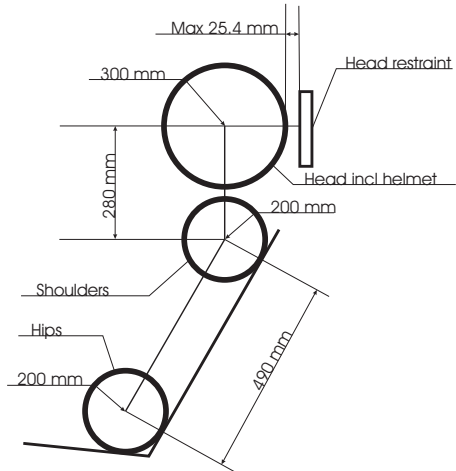


Figure 6.1: 95th percentile male driver template

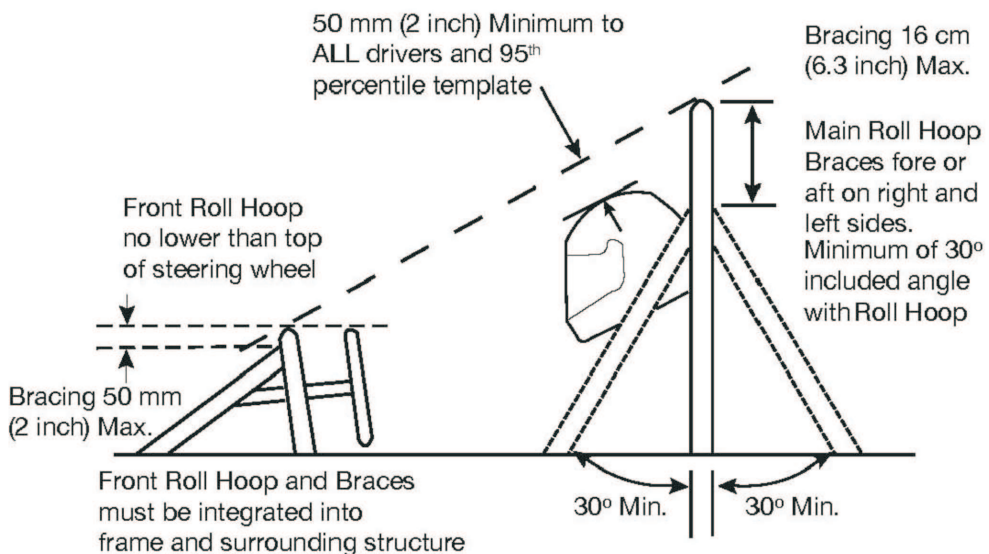
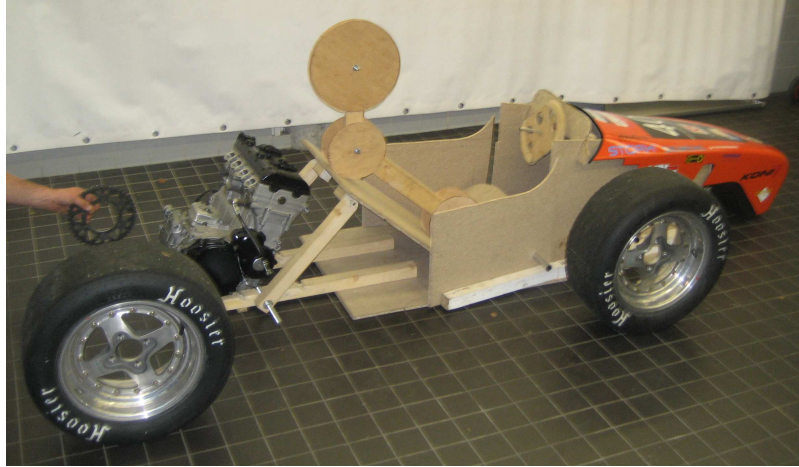


Figure 6.2: Geometric rules considering the front and main roll hoops



(a)



(b)

Figure 6.3: A wooden mock-up and the URE04 are used to analyse the driver ergonomics

Chapter 7

Final design

Combining all that has been mentioned so far with the design tools from Chapter 8 a final design has emerged. It has been an iterative process of which the final results are presented in this Chapter.

In Figure 7.1 the final design is presented in an exploded view. What can be seen immediately is the application of the Multi-Shell Assembly Approach consisting of side shells and a top and bottom shell. These two side shells form the structural monocoque and consist of sandwich panels. The top and bottom shell consist of only a few plies of CFRP. Furthermore the nose cone is shown which is being implemented in another project to form a crash impact attenuator. At the rear a simple tubular frame has been designed that supports the rear suspension and the engine. They aluminum rear bulkhead completing the rear frame is designed outside the scope of this report. The main and front roll hoops are shown in the figure as well. Note that the main roll hoop is integrated in the rear frame.

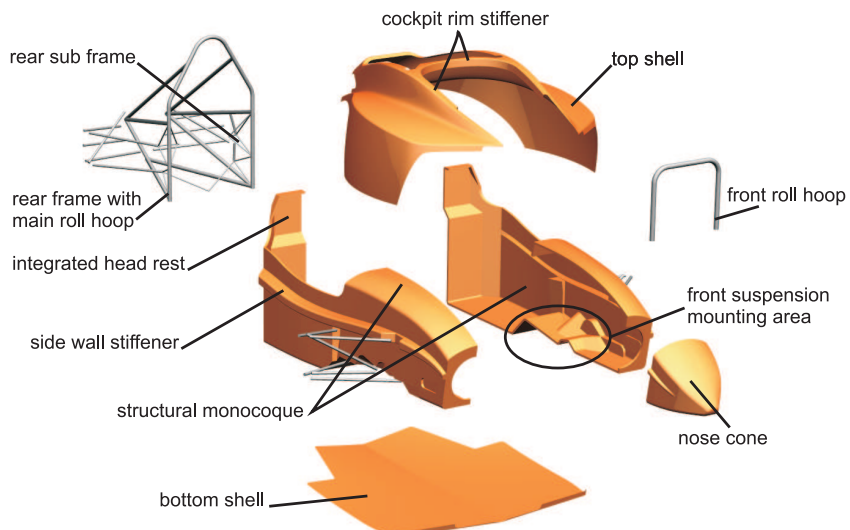


Figure 7.1: An exploded view of the final design using the Multi-Shell Assembly Approach

The structural monocoque deserves some more explanation. It consists of sandwich panels with 10 mm Rohacell® 71 IG core and $45^\circ/0^\circ/-45^\circ/90^\circ$ laminates of u.d. plies on either side. Woven plies could be used instead to improve the manufacturing ease. One can see that the chassis bulges up in the area of the front suspension. This is done so the suspension system can be mounted on the outside of the car. This allows for the components to be reachable at all times and it lowers the center of gravity because of the quite significant masses of the suspension system. Taking a close look one can see all the separate surfaces that have been designed. These are all mounting surfaces for the different connection rods, rockers etc. All these surfaces are made in such a way that the component arrives at that surface under an angle of 45° making the force application more smooth.

In addition one can see that all the surfaces where important components are mounted to the chassis are supported in such a way that the force is absorbed by sandwich plates that are loaded in the right way - i.e. they are loaded in-plane. In most cases this means that a small mounting surface is created surrounded by surfaces in the right direction that guide the applied forces away from the loading point. An example of this is the side wall stiffener that flows across the side of the monocoque (Figure 7.2). This stiffener supports both the upper front suspension points and makes for an important part of the side impact area (see section 8.8). The mounting bracket that is seen on Figure 7.2 is designed separately and is not discussed here. Note also the folded dashboard to give the open edge over the top bending stiffness. The head rest has also been integrated in the monocoque.

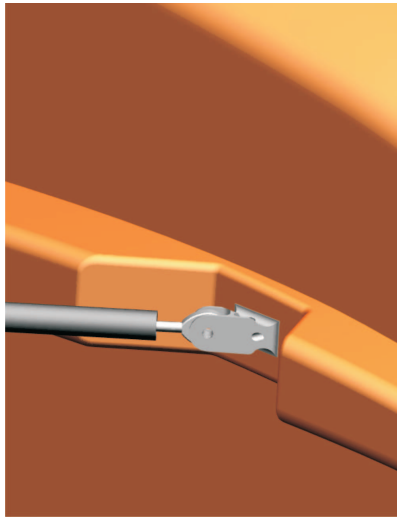


Figure 7.2: Detail of the suspension mounting point at the side wall stiffener

The bottom shell is a straightforward plate that covers the bottom of the rear frame to protect the engine compartment from road rubble etc that is disturbed and thrown up by the front tires. In addition it closed the bottom of the side pods.

The top shell is slightly more complicated. The most important structural part is the cockpit rim stiffener. The top shell falls into the monocoque along the cockpit sides and goes over the edge towards the outside, creating a spacious profile. This is illustrated in detail in Figure 7.3. In Chapter 8 the influence on the torsional stiffness of adding the top shell is shown. Furthermore the major part of the side pods is formed by the top shell.

The rear frame consist of the main roll hoop, the main frame and a sub frame to mount the rear suspension. The engine is mounted to the rear bulkhead as well as the sub frame while the suspension connects to the rear bulkhead and the subframe. This is shown in more detail in Figure 7.4 as well as the mounting areas to bolt the rear frame to the chassis. These mounts have been designed parallel to this report and are not discussed here.

All four main parts are manufacturable requiring only one mold each. One might consider manufacturing the molds from several parts because of the size though and an additional mold is needed for the nose cone. The manufacturing process however is rather straightforward and combining the four shells with the nose cone and the rear frame, one comes to the final design: a lightweight hybrid race car chassis consisting of a fiber reinforced composite monocoque combining structural, esthetic, ergonomic and crash properties, and a tubular space frame engine compartment, meeting stiffness and strength demands, which is fairly simple to produce. Structural and crash properties are evaluated in the next Chapter and regarding the aesthetics, see for yourself: Figure 7.5.

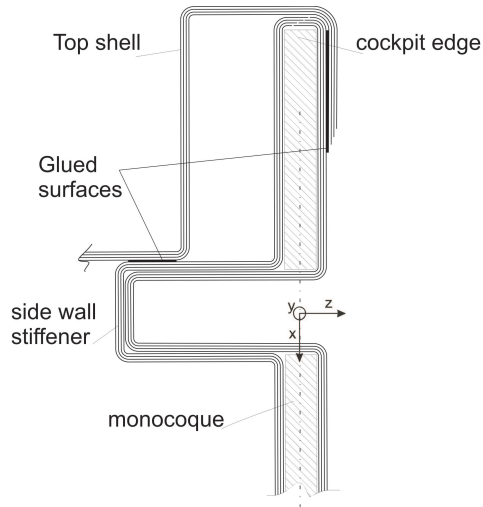


Figure 7.3: Detail of the cockpit rim and side wall stiffener, the top shell is glued to the monocoque creating an spacious profile

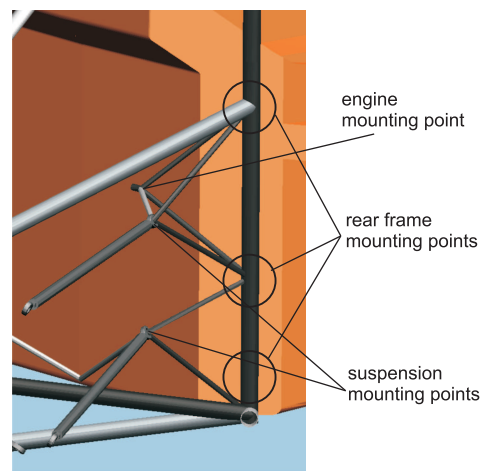


Figure 7.4: The rear subframe that holds part of the rear suspension and the engine



Figure 7.5: The final design

Chapter 8

Stiffness and strength analysis

In this Chapter the final results for the stiffness and strength analysis are presented. A model is presented to analyse the torsional stiffness and total mass and the results are compared to the design goals. Two methods have been used to meet these goals. Firstly, the geometric efficiency, to remove local stress peaks due to inefficiencies in the material allocation. Secondly eigen modes analysis identifies weak spots regarding specific stiffness and it is used to advise on further improvements.

Failure initiation typically occurs around hardpoints - i.e. points where loads enter the chassis, often transversely. A model has been set up to investigate the influence of several measures mentioned in section 4.9 to reduce stress localization and a detailed model is used to look at the stresses occurring in the current design.

The tubular rear frame is examined to advise on the required geometry and material of the tubes and finally for several areas on the monocoque, the rules state that from a safety point of view, the structure must equivalent to a certain steel tubular frame. Calculations are made to show that the current design can meet those demands.

Analysis has been done using Altair Hyperworks[®] for meshing and global calculations, MSC Marc/Mentat[®] for detailed calculations and Matlab[®] to process most results.

8.1 Torsional stiffness

The model is build up in Altair Hyperworks using 2D plane stress shell elements for the monocoque, 1D beam elements for the tubular rear frame and the connection rods and 3D solid elements for the rear bulkhead. The connection rods are 3 DOF attached to the monocoque, rear frame and rear bulkhead simulating rigid ball joints. The wheel hubs are modeled as rigids as well as all the mounts of the rear frame to the monocoque and rear bulkhead. The model is shown in Figure 8.1. The monocoque laminate is built up from 10 mm of Rohacell[®] 71 IG with faces of 45°/0°/-45°/90° 0.2 mm plies of u.d. CFRP's. The rear frame consist

of mild steel and the rear bulkhead of aluminium. Furthermore the connection rods of the suspension are modeled as tubular profiles of u.d. CFRP oriented in the direction of the rod center lines and plywood inserts are used. The properties of the materials used in this model are found in Chapter 4.

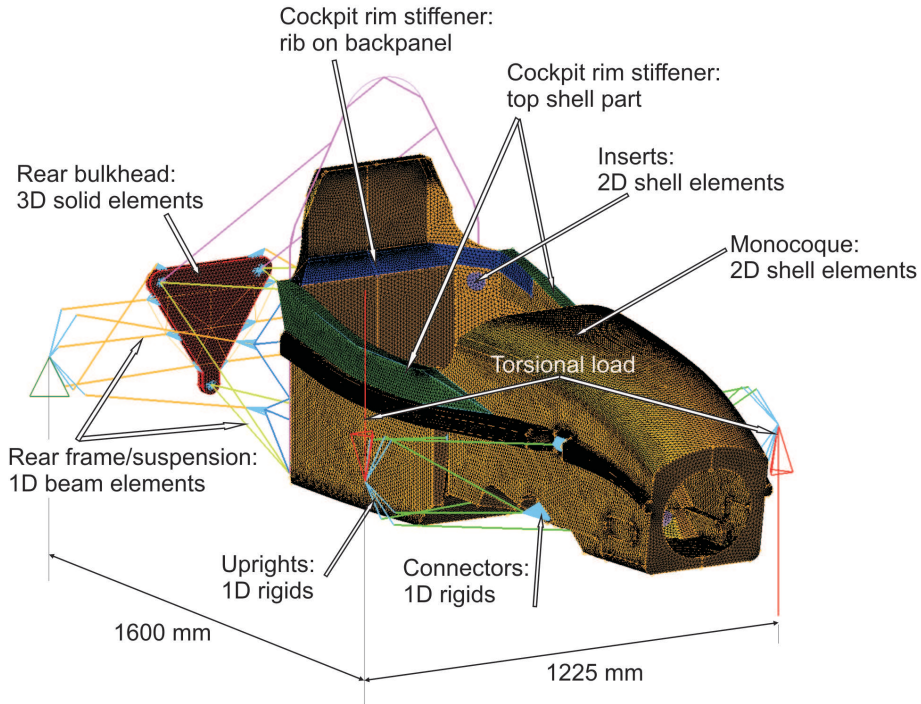


Figure 8.1: The model set up in Altair Hyperworks®

A vertical load of 10 kN is applied to both the front wheel centers in opposite direction to simulate the torsional load while the rear wheel centers are constraint. This appears to give the most realistic results considering the analogy with the real torsional load. In addition the stiffness of the connection rods is added to the equation. Two situations are evaluated: the structural monocoque by itself (Figure 8.2a) and the structural monocoque with the cockpit rim stiffener added (Figure 8.2b), to show the influence on the stiffness of adding the rim stiffener. Note that this rim stiffener consists of a rib over the back panel as well as the top shell part glued over the rim and to the side stiffener.

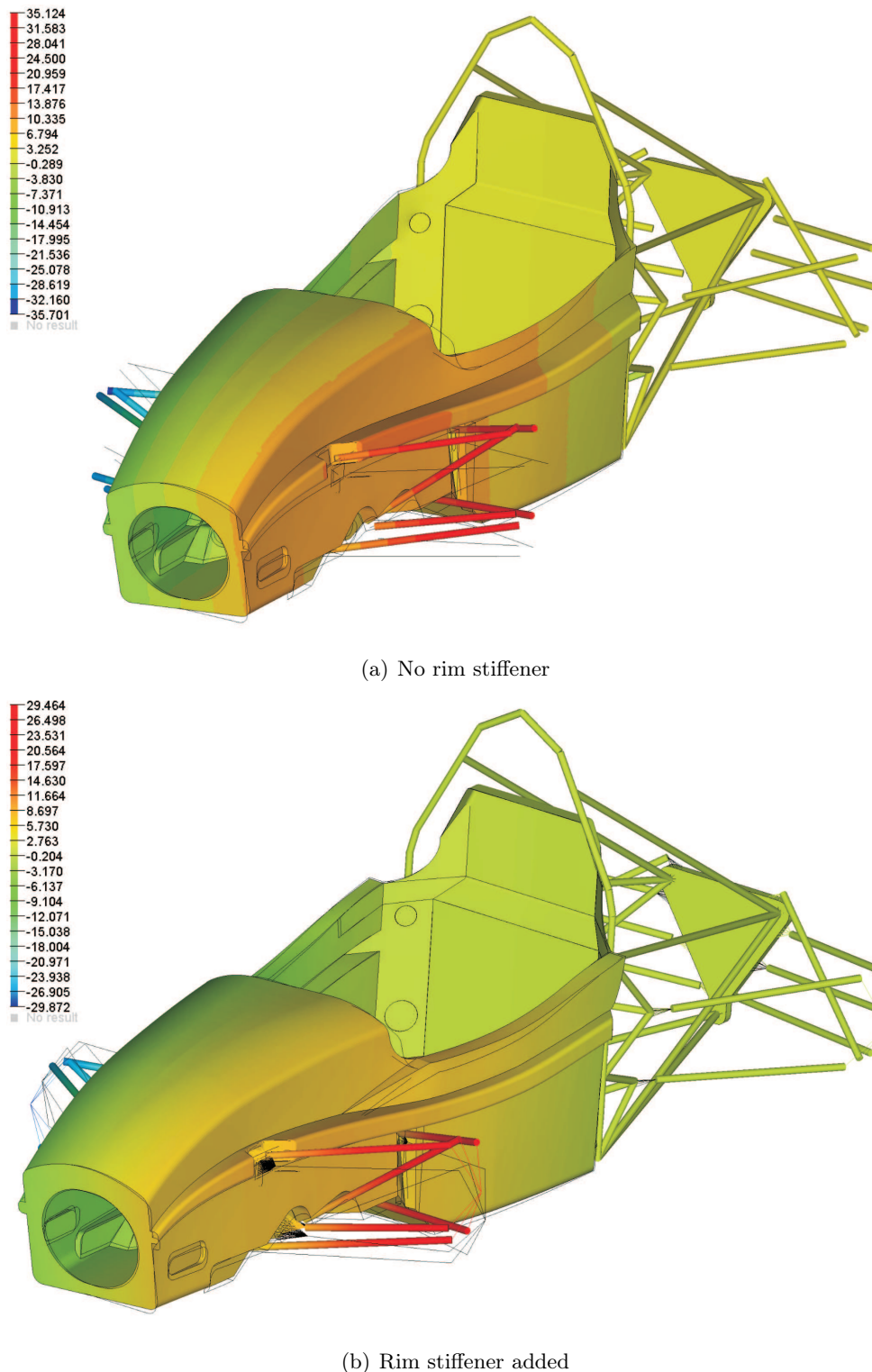


Figure 8.2: Vertical displacement in mm under a torsional

To calculate the torsional stiffness, the average vertical displacements of the front right and left wheel centers Δz is taken from Figure 8.2b. These are combined with the torsional load which results in:

$$k = \frac{M}{\beta}$$

with the torsional moment $M = 2Fl$

and the angular deflection $\beta = \tan^{-1}(\frac{\Delta z}{l})$

$$k = \frac{2Fl}{\tan^{-1}(\frac{\Delta z}{l})} \approx 260 \text{Nm/rad}$$

With $F = 10 \text{ kN}$, $l = 0.6125 \text{ m}$ (half the trackwidth) and $\Delta z \approx 29$.

8.2 Specific stiffness

Using Altair Hyperworks® the total weight of the analyzed model can be calculated. Although some additional material will be added at certain places, the calculation from Hyperworks® is a very good indication. Combining the weight of the CFRP sandwich panel monocoque, the wooden hardpoint inserts, the steel main roll hoop, the rear steel tubular frame and the aluminum rear bulkhead, a total weight of approximately 22 kg is found. A comparison of the calculated specific stiffness with the set design goals is shown in Table 8.1.

	mass	stiffness	specific stiffness
URE05 chassis targets	<25 kg	>200 kNm/rad	>8 kNm/rad/kg
URE05 chassis calculated	22 kg	260 kNm/rad	11.8 kNm/rad/kg

Table 8.1: Current status of torsional stiffness in Formula Student race cars

8.3 Stress peaks due to geometrical inefficiencies

Using the torsional model the stresses are evaluated using the Hoffman criterium. For all plies of CFRP the global failure indices are calculated, these are not shown here because of sheer amount of data involved. In general the criteria are met easily for the torsional loadcase regarding global ply failure and the method has been used specifically to detect stress peaks and critical areas. Regarding geometric inefficiencies, around corners, sharp edges, and geometric changes close to the hardpoints, stresses typically rise to unacceptable levels. By smoothing the geometry - i.e. by removing discontinuities - most of these local stress rises due to geometric inefficiencies have been accounted for. One problem area still remains however. This is the area under the legs of the driver where the front suspension system is mounted close to the gluing seam of the two halves of the monocoque. In Figure 8.3 the problematic area is shown. This must be dealt with by applying ply strengthening - i.e. locally reinforcing the sandwich faces. In addition the plywood insert can be extended over the seam to take part of the load and the mounting bracket must be of a bridge like shape connecting the suspension mounting points on both sided of the seam, carrying the load over the seam.

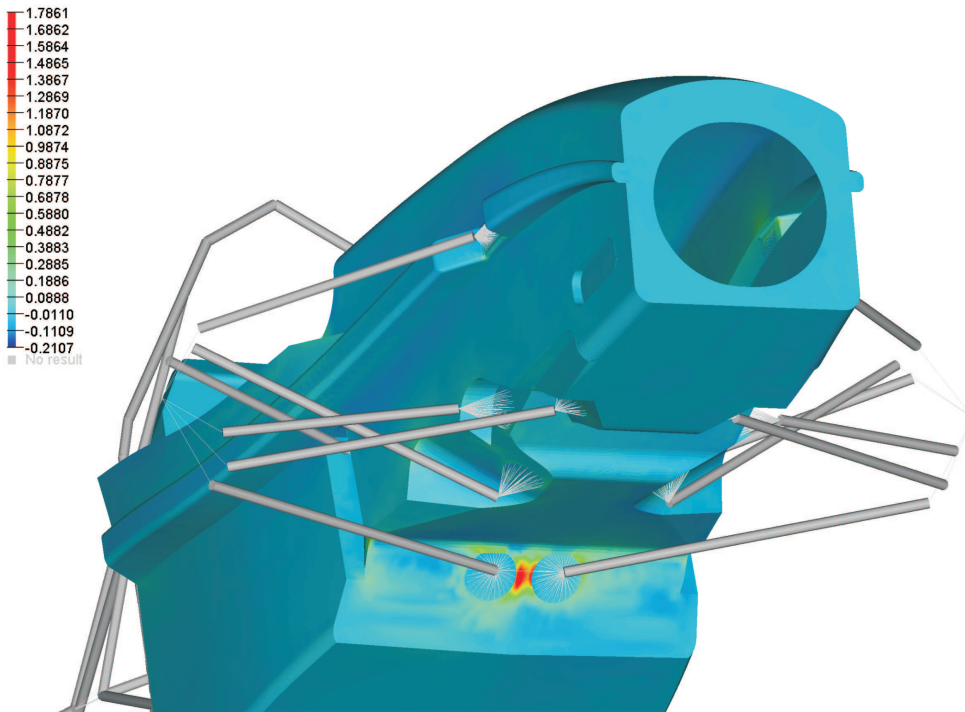


Figure 8.3: Hoffman failure index in one of the plies for the remaining problem area in the design due to high stress localization in the vicinity of a gluing seam.

8.4 Eigen mode analysis

The first eigen mode of a structure are determined by $\sqrt{k/m}$ which means that they are a convenient measure for the specific stiffness of the structure. It allows for quick identification of areas where either stiffness is required or where mass can be removed. This has been an important tool in achieving the high specific stiffness presented in section 8.2.

The first eigen frequencies have been analyzed using an expanded version of the torsional model from section 8.1. With all four wheels constrained and the load removed, any number of eigen modes can be extracted from it. They first modes are all under 10 Hz, which is important because the engine constantly excites the chassis at frequencies above 25 Hz. Furthermore the lateral frequencies of a typical Formula Student slalom lie between 1 and 3 Hz so the torsional and lateral eigen frequencies of the chassis are designed to be between 5 and 10 Hz. Problem areas such as the cockpit rim and the front suspension mount could be evaluated and measures such as the cockpit rim stiffener and the side wall stiffener were implemented using eigen mode identification. Other interesting areas that been improved severely due to eigen mode analysis are for instance the head rest and the dashboard (which functions as a stiffener for the top side of the monocoque front).

A problem area that still remains difficult to tackle is the most forward upper front suspension mount. A known solution is to glue bulkheads in the cockpit to stiffen these areas. However there is hardly any room to add material because of the internal cockpit dimensions regulations (Appendix B) and it was mentioned earlier that the number of parts is to be kept at a minimum. Already it has been severely improved using the side wall stiffener but other measures could be taken still in the manufacturing process. It is suggested to fill the rib locally with foam and add additional plies on the inside of the rib to further stiffen this area. In Figure 8.4 the eigen that identifies this area is shown and in Figure 8.5 the way to fill the rib is shown.

Another problematic area that was already identified from the start is the cockpit rim. By properly gluing the top shell to the structural monocoque the stiffness is already improved severely. Considering however that the second eigen mode is dominated by the compliance of the cockpit rim (Figure 8.6) it remains an area of interest. A suggestion to improve it even further during the assembly process is to glue foam in between the surface of the top shell and the monocoque as shown in Figure 8.7.

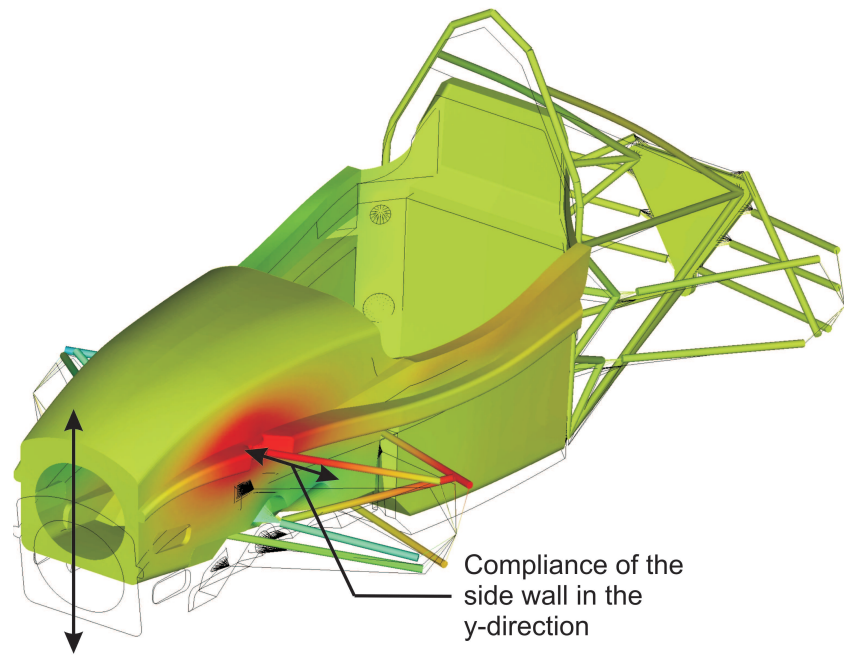


Figure 8.4: The eigen mode (magnitude is shown in the y-direction, $f = 2.6\text{Hz}$) that occurs due to compliance around the front suspension mount at the side wall stiffener.

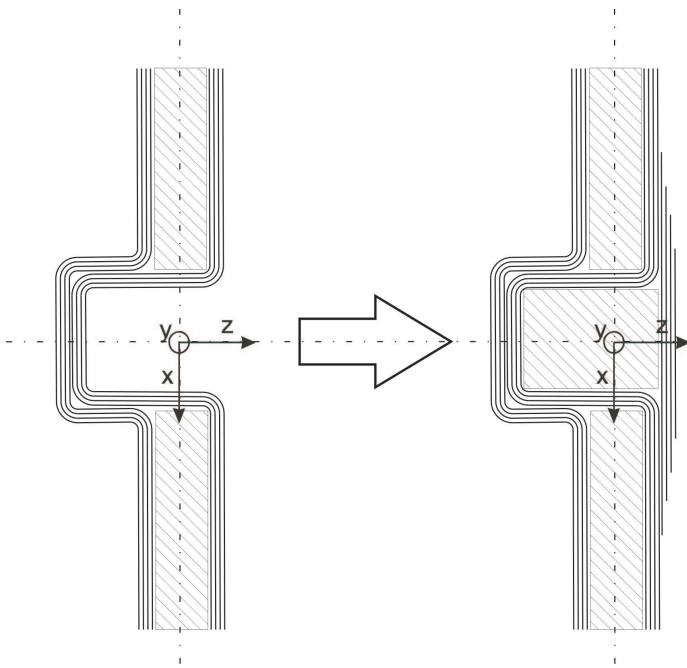


Figure 8.5: By filling the side wall rib with foam and adding plies on the inside of the chassis it can be made less compliant.

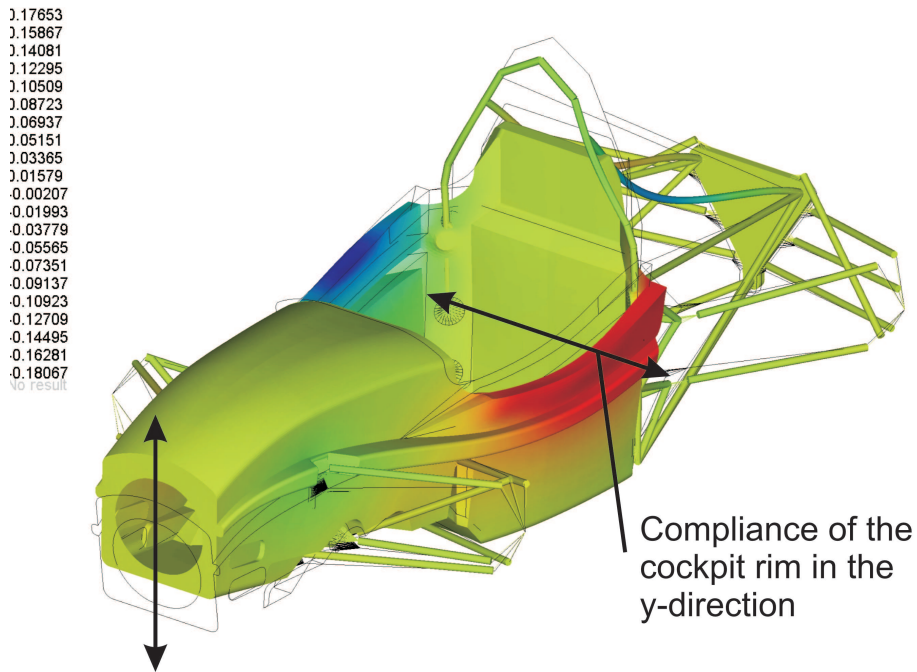


Figure 8.6: The eigen mode (magnitude is shown in the y-direction, $f = 3.2\text{Hz}$) that occurs due to compliance of the cockpit rim.

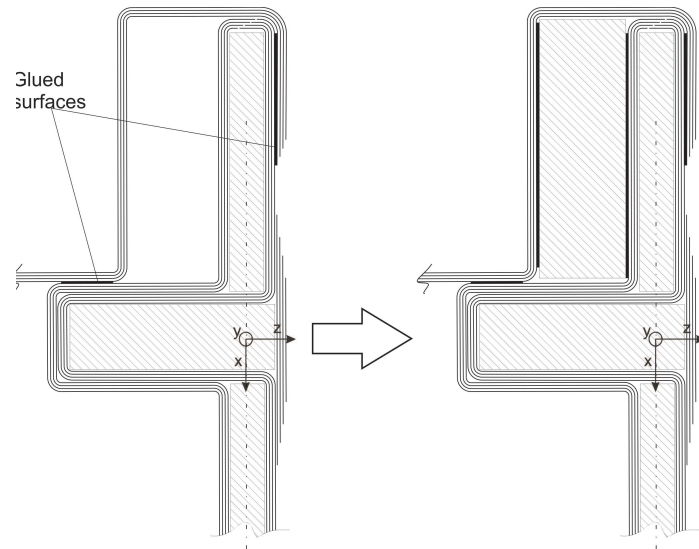


Figure 8.7: By filling the area between the sandwich structure and the top shell with foam during assembly it can be made less compliant.

8.5 Hardpoint analysis

The strength of the hardpoints is determined by two material discontinuities, the discontinuity due to the mounting bracket and the one caused by the insert/core junction. The stresses across the insert/core boundary and around the edges of the mounting bracket are evaluated using FEA models. Different scenario's are used to show the influence of the measures to reduce stress localization. These scenario's for the current design, shown in Figure 8.8, are :

- A: a straight insert with a straight and rigid mounting bracket
- B: a straight insert with a straight and rigid but glued mounting bracket
- C: a straight insert with a compliant/tapered and glued mounting bracket
- D: a tapered insert with a compliant/tapered and glued mounting bracket

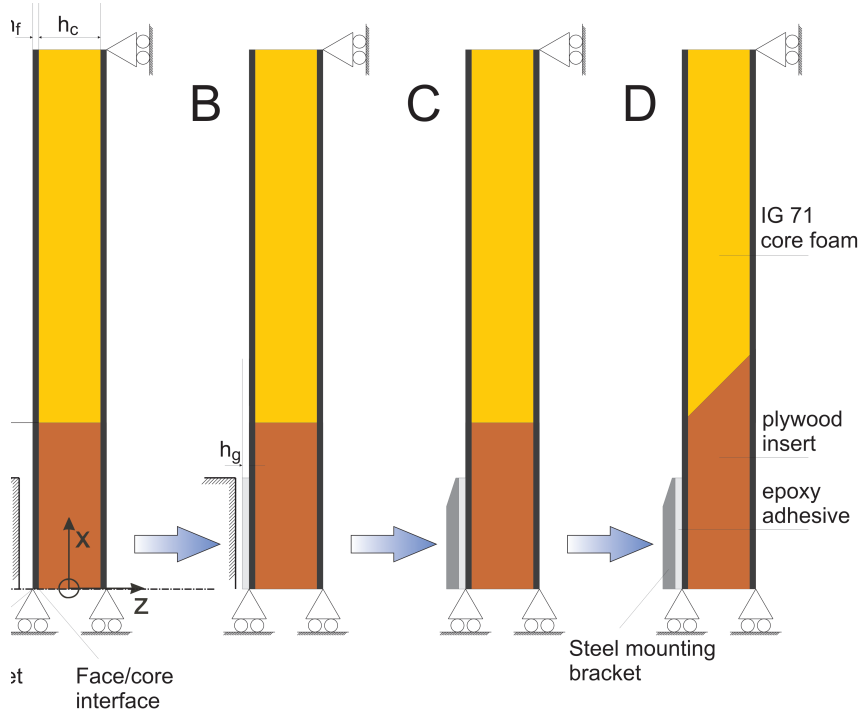


Figure 8.8: The scenario's for the current design modeled in MSC Marc/Mentat[®], $h_f = 1$ mm, $h_c = 10$ mm, $h_g = 0.2$ mm, $r_o = 25$ mm, $r_m = 17.5$ mm

The materials used are as presented in Chapter 4. The CFRP is modeled as a quasi-isotropic material equivalent to a $45^\circ/0^\circ/-45^\circ/90^\circ$ lay-up with 0.2 mm layers - i.e. $h_f = 0.8$ mm. Again the cheapest available core is used, Rohacell[®] 71 IG with $h_c = 10$ mm, and Birch-plywood is used for the 50 mm insert - i.e. $r_o = 25$ mm. A steel mounting bracket with radius $r_m = 17.5$ mm and 1 mm thickness sits on top of a 0.2 mm layer of epoxy adhesive glue. For convenience this epoxy is assumed to be equal to the epoxy in the prepreg CFRP's. The used material

properties are presented in Table 8.2.

	Plywood	71 IG	CFRP	Steel	Aluminum	Epoxy
E_x [N/mm ²]	7070	92	56300	210000	70000	2500
E_y [N/mm ²]	7070		56300			
E_z [N/mm ²]	1130		11200			
ν_{xy} [-]		0.3		0.3	0.3	0.3
ν_{xz} [-]						
ν_{yz} [-]						
G_{xy} [N/mm ²]	530		21720			
G_{xz} [N/mm ²]	130		4660			
G_{yz} [N/mm ²]	130		4660			

Table 8.2: Material properties used in the hardpoint analysis

The models used to analyze these scenario's are built in MSC Marc/Mentat®. They consist of simply supported axi-symmetric models of a circular insert. In this way a 3D analysis can be done with a 2D mesh, simplifying the model severely and thus reducing calculation time. 2D quadratic elements are used because they describe bending behavior much better compared to first order elements. For now a fixed displacement of 3mm is applied to the mounting bracket to evaluate the effects of transverse loading. A contact is simulated between the mounting bracket, the layer of epoxy adhesive and the plies of CFRP. The stresses of relevance - i.e. normal stresses σ_x and σ_y , peel stress σ_z and shear stress τ_{xz} - are analyzed on the face/bracket interface and the face/core interface because on these interfaces failure typically initiates. To obtain the results the stresses are calculated at the Gaussian points and extrapolated to the element nodes. The difficulties in analyses across material discontinuities can be partly solved by making the mesh elements small enough. An example of such a mesh is given in Figure 8.17.

The results of the face/bracket interface for the four scenario's are shown in Figures 8.9 to 8.12. The effects of delocalization on the height and distribution of the stresses can be seen clearly:

1. Severe reduction of the peak stress on the mounting bracket edge ($x = r_m$) due to the application of a 0.2 mm layer of glue and a compliant bracket
2. Strong delocalization of the stress due to the application of a 0.2 mm layer of glue and a compliant bracket
3. Severe reduction of the local effects across the insert/core boundary ($x = r_o$) due to tapering of the insert

In addition some major local effects can be seen around $x = 6.5$. This is due to the fact that the displacement is forced upon the nodes up to $x = 6.5$. This creates another discontinuity and thus peaks in the stresses. Considering the properties of each material the normal stresses σ_x and σ_y are taken up by the tensile and compressive strengths of the CFRP plies. For $x \leq 17.5$ the normal stress σ_z and shear stress τ_{xz} however must be absorbed into the epoxy adhesive that bonds the

outer ply to the mounting bracket. For $x \geq 17.5$ mm the limiting factor is the epoxy that bonds the fibers.

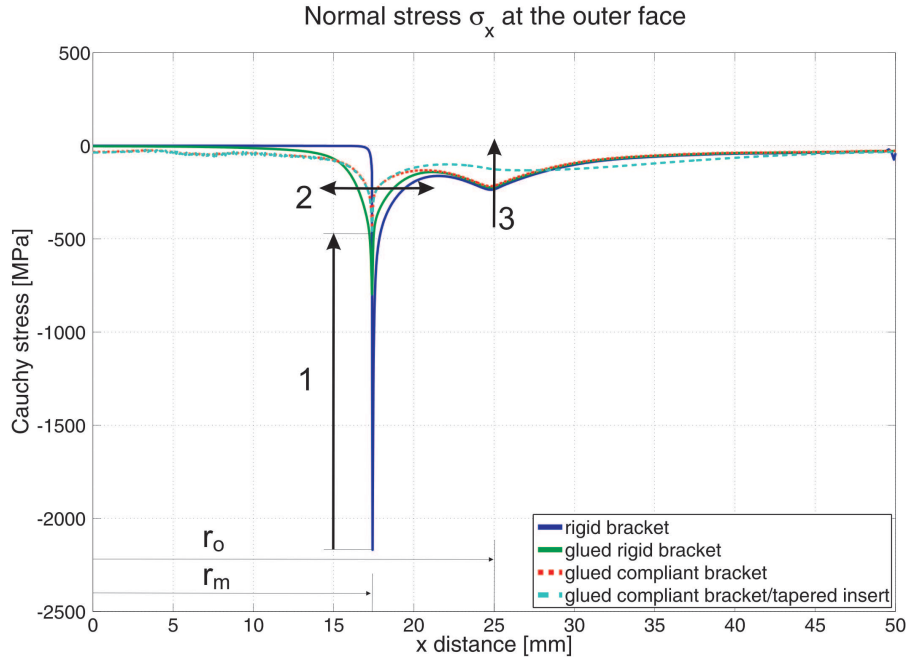


Figure 8.9: Effects of in-plane stress delocalization on the face/bracket interface for the four scenario's

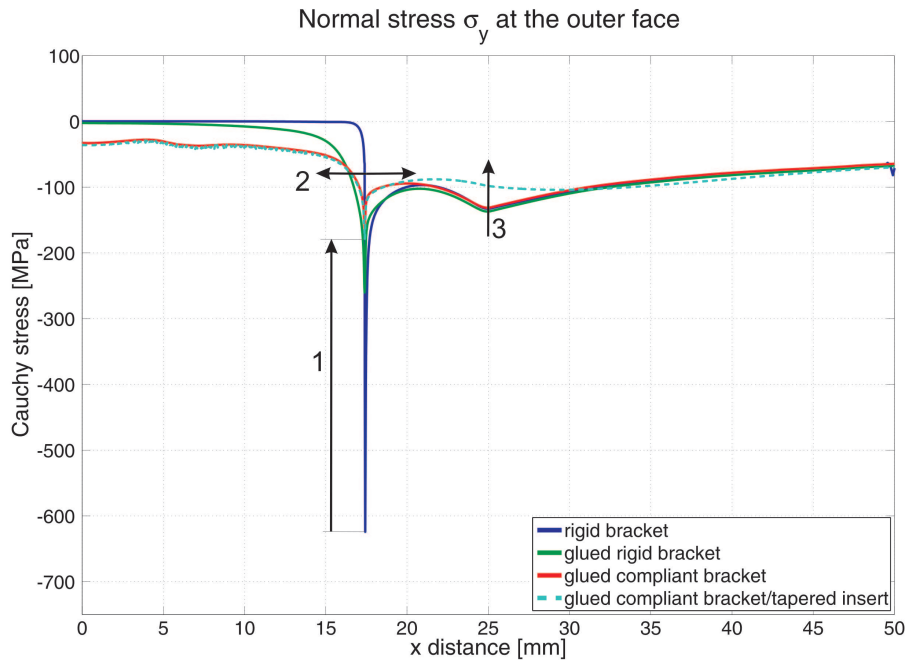


Figure 8.10: Effects of in-plane stress delocalization on the face/bracket interface for the four scenario's

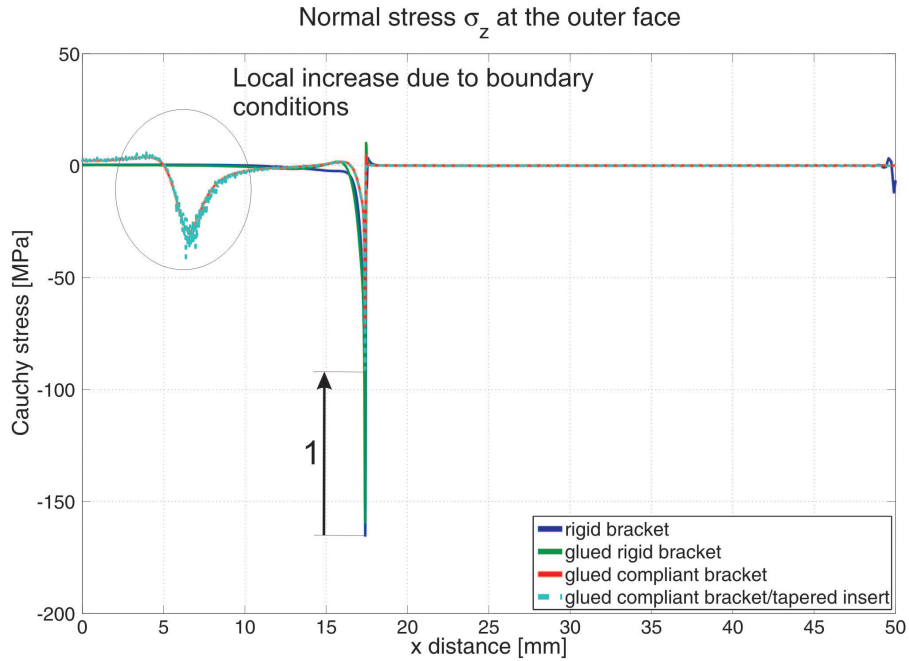


Figure 8.11: Effects of transverse stress delocalization on the face/bracket interface for the four scenario's

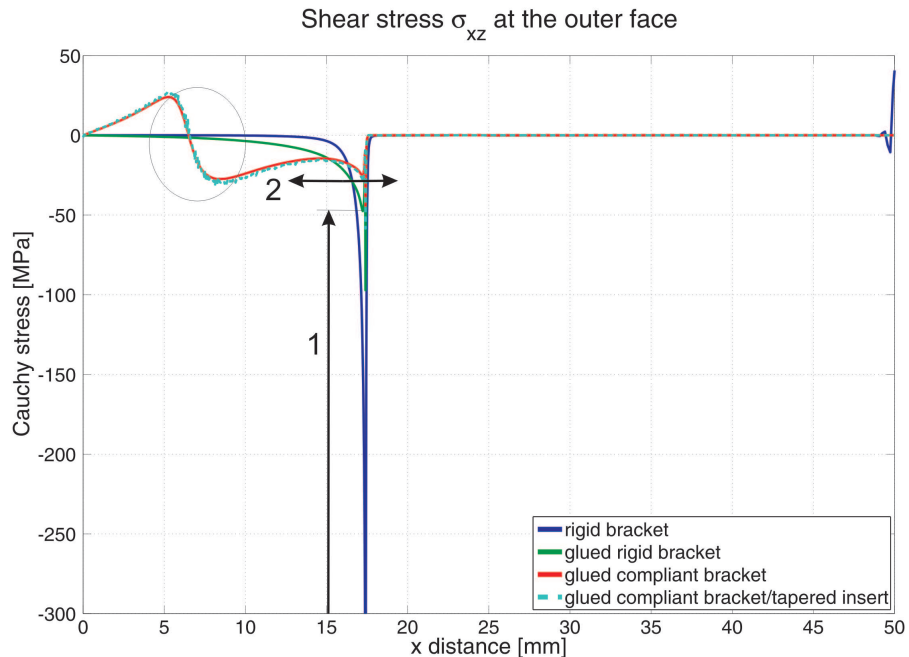


Figure 8.12: Effects of shear stress delocalization on the face/bracket interface for the four scenario's

For the face/core interface a different picture is seen (Figure 8.13 to 8.16). One can again see a huge reduction in peak stresses due to a compliant mounting bracket and tapered insert. Due to the overall lower stresses however, the local effects due to the boundary conditions become more dominant. In reality however these effects are far less due to the more gradual introduction of the force into the mounting bracket.

Again the normal stresses σ_x and σ_y are absorbed by the CFRP plies. The peel and shear stresses at $x = r_m$ are absorbed by the tensile strength of the epoxy and the transverse compressive strength of the plywood insert. At $x = r_o$ however the critical strength becomes the tensile and shear strength of the foam core.

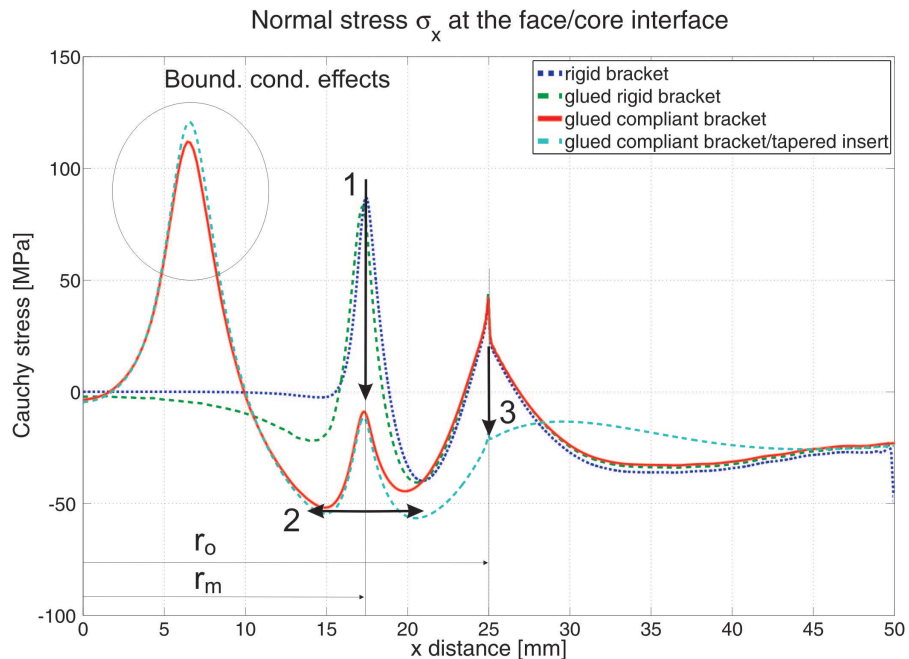


Figure 8.13: Effects of in-plane stress delocalization on the face/core interface for the four scenario's

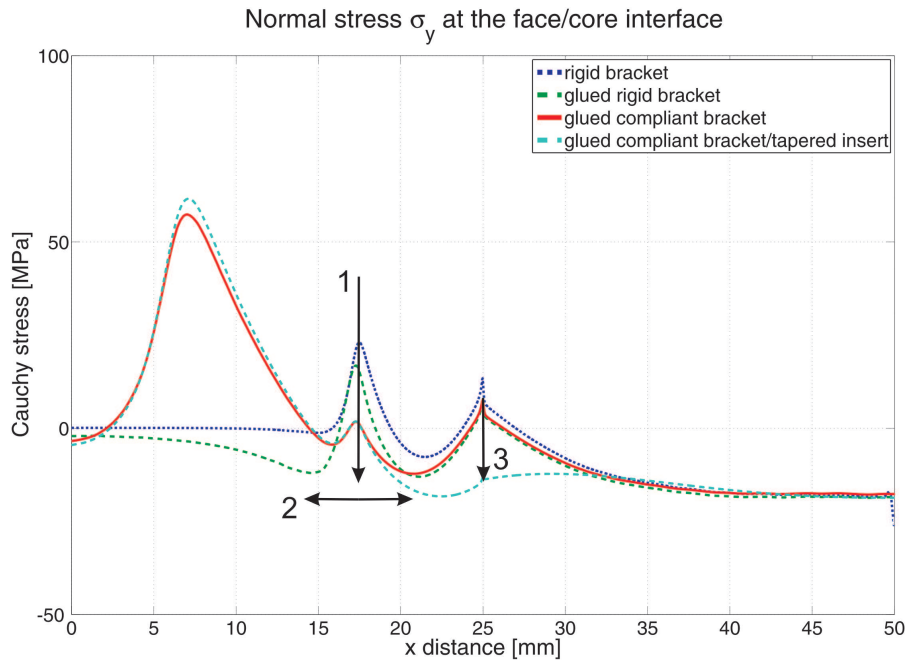


Figure 8.14: Effects of in-plane stress delocalization on the face/core interface for the four scenario's

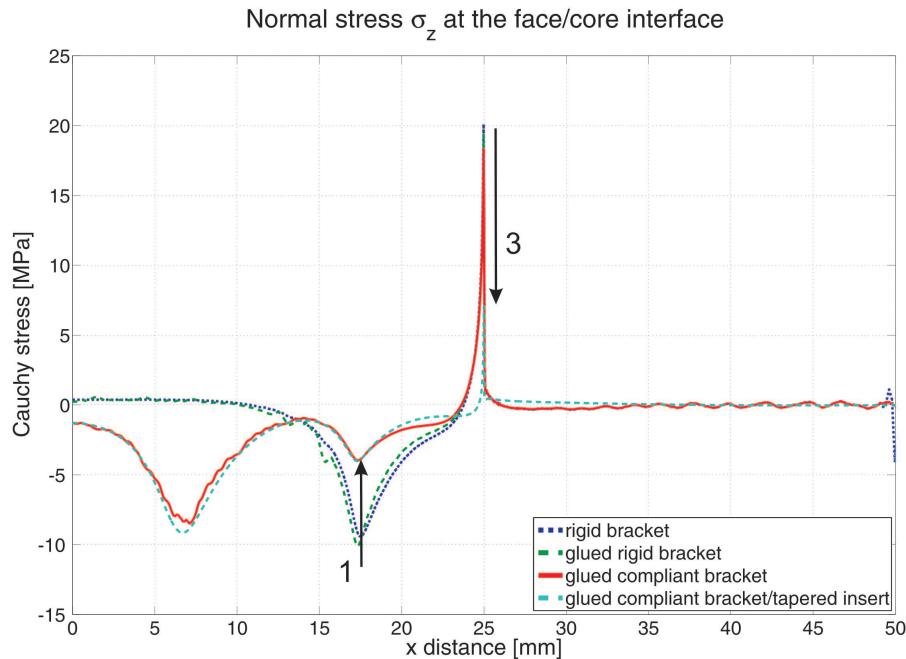


Figure 8.15: Effects of transverse stress delocalization on the face/core interface for the four scenario's

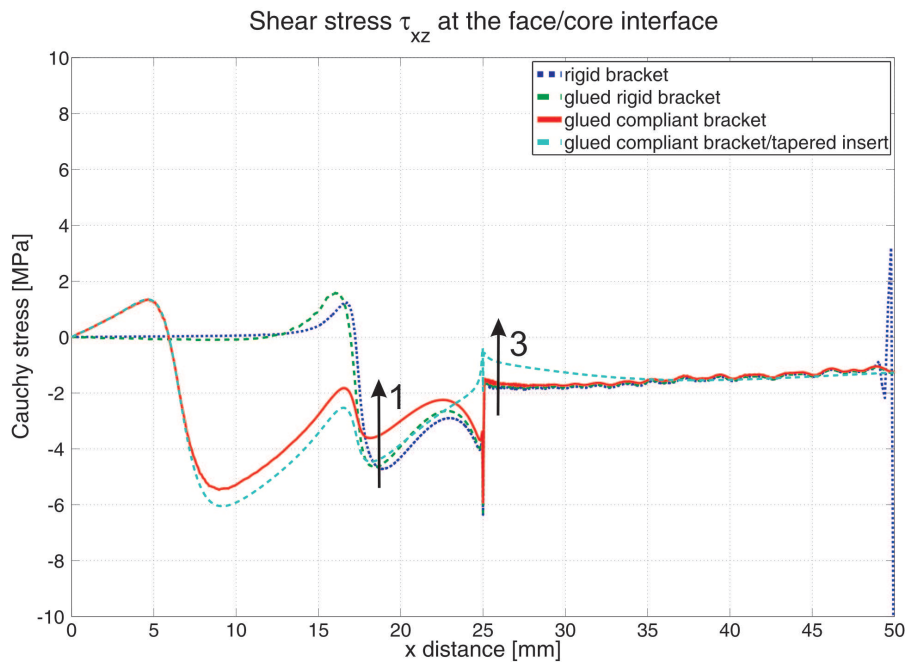


Figure 8.16: Effects of shear stress delocalization on the face/core interface for the four scenario's

Now that the effects of stress delocalization measures have been shown on the two critical boundaries, the final design is examined further. The model consists of scenario four from Figure 8.8, expanded to a dubbel sided compliant mounting bracket glued to the outer faces. A transverse as well as an in plane force are applied to the outer mounting bracket. The model as well as its mesh are shown in Figure 8.17.

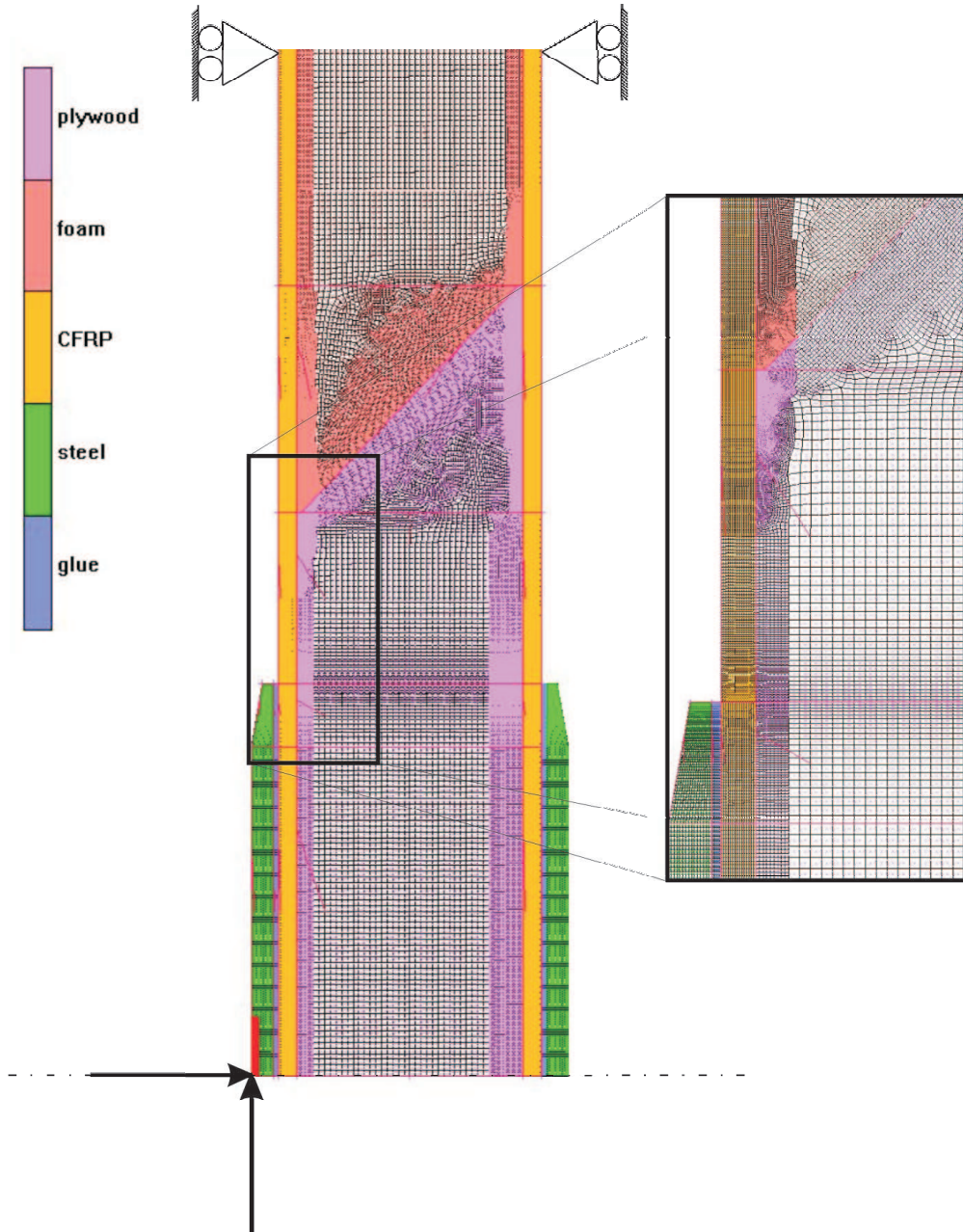


Figure 8.17: The model created in MSC Marc/Mentat® for the final model

The results for the face/bracket and face/core interfaces on both sides are shown in Figures 8.18 to 8.21. In these figures the relevant maximum allowable stresses for an u.d. ply of CFRP, the epoxy adhesive and the foam core from Chapter 4 are identified. The relevance of the allowable stress depends on the fact that for the different stress peaks at the different discontinuities other materials are critical with respect to failure initiation. This is beneficial because it also allows for specific local solutions to further reduce the local stresses. Note in addition that the peaks at the discontinuities are partly caused by numerically discontinuities, especially at the bracket edge.

$\sigma_{x_{max}}$: The maximum stress does not exceed either maximum compressive or tensile strengths.

$\sigma_{y_{max}}$: The tensile stress is critical for u.d. layer of CFRP. Therefor a woven or a 90° u.d. ply is added to locally strengthen the laminate to distribute both the x- and y-component of the stress smoothly into the laminate.

$\sigma_{z_{max}}$: The peel stress peaks severely at backside of the laminate along the mounting bracket edge. In fact it shows a similar pattern as that of the rigid bracket in Figure 8.11. It is therefore advisable to machine the bracket to be as thin as possible, especially along its edge. Another measure to decrease the peel stress is to make sure the adhesive is thick enough and choosing an adhesive with low E [8]. In manufacturing the adhesive must be applied very carefully to create a smooth tapering of the adhesive along the bracket edge. Local peaks are also seen across the insert/core boundary. Here the tensile and compressive strength of the core becomes very critical. In practice, there will be a little space between the insert and core material. This will be filled with epoxy during the manufacturing process. This acts as a buffer reducing the local stresses [9]. Also the above suggested ply strengthening will reduce these peaks.

$\tau_{xz_{max}}$: Again at the bracket edge, the peaks are disturbing. Taking the measures mentioned above will reduce the peaks however it is advisable to apply core patching at the hardpoint that are loaded the strongest. The WF 200 variant of Rohacell shows very promising properties.

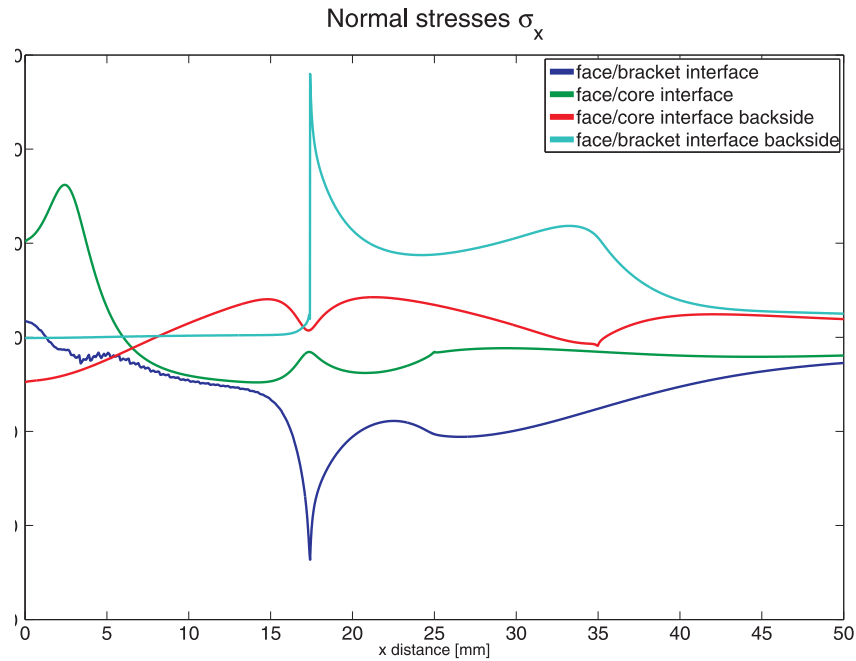


Figure 8.18: The stresses in x-direction are very acceptable for u.d. plies

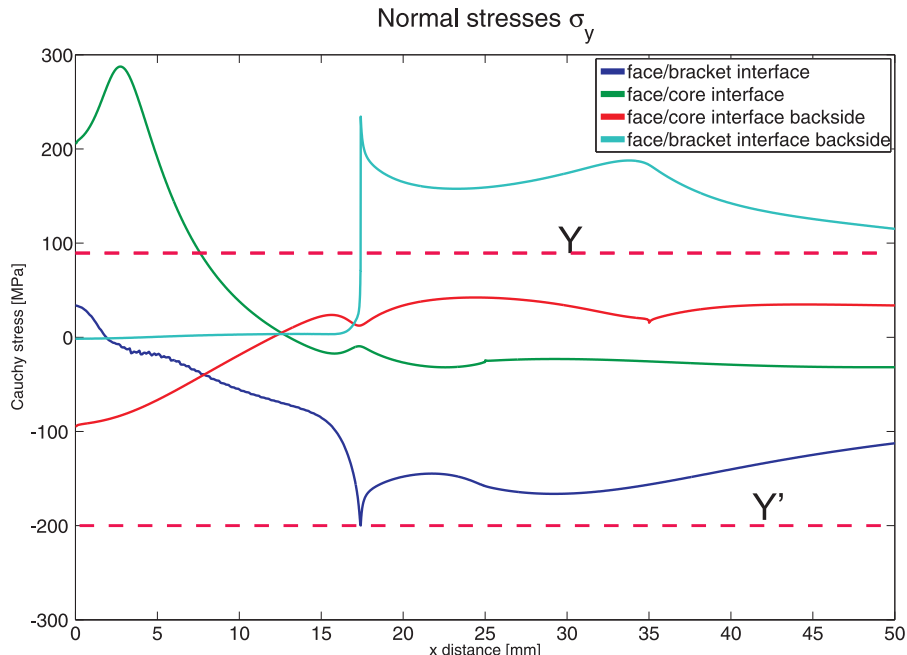


Figure 8.19: The tensile stresses in the y-direction exceed the allowable stress for Y for u.d. plies

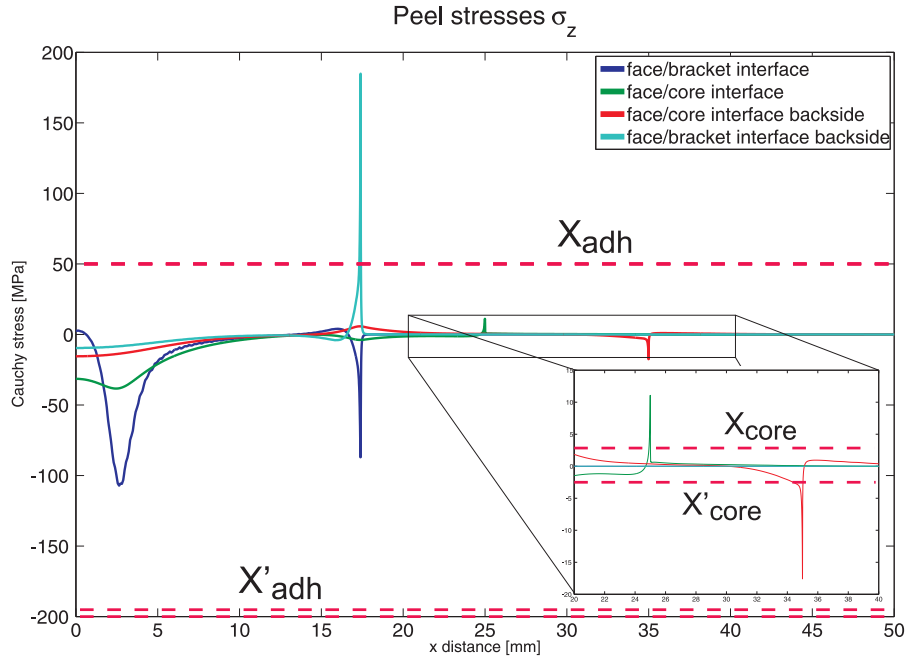


Figure 8.20: The peel stresses in the adhesive X_{adh} and the core X_{core} are critical as well as the compressive strength of the core X'_{core}

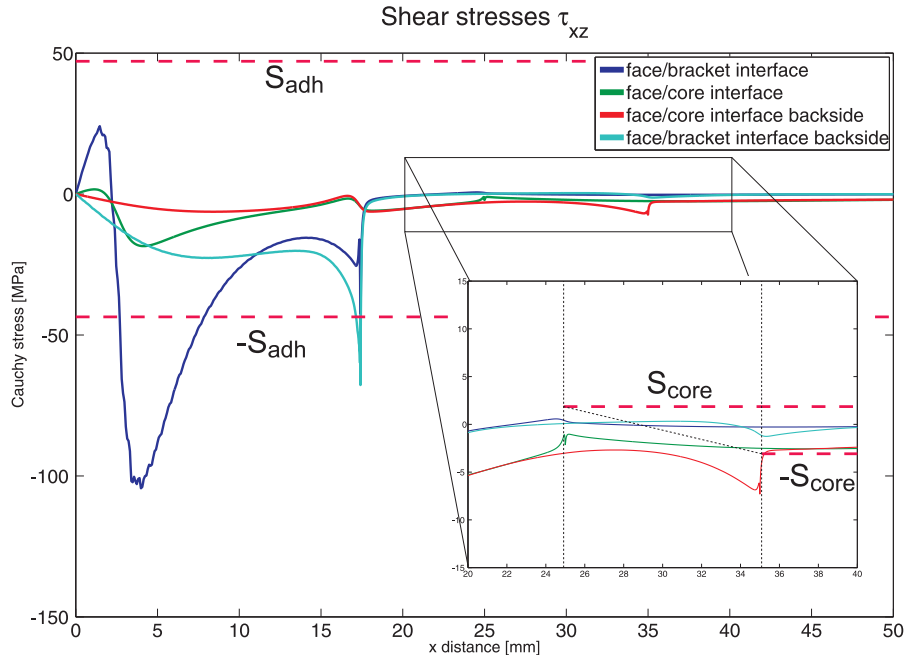


Figure 8.21: The shear stresses of both the adhesive S_{adh} and the core are critical S_{core}

8.6 Rear frame tension and buckling

From the torsional model the stresses in the rear frame can be evaluated as well. These stresses are shown in Figure 8.22. In the model the tubes have an

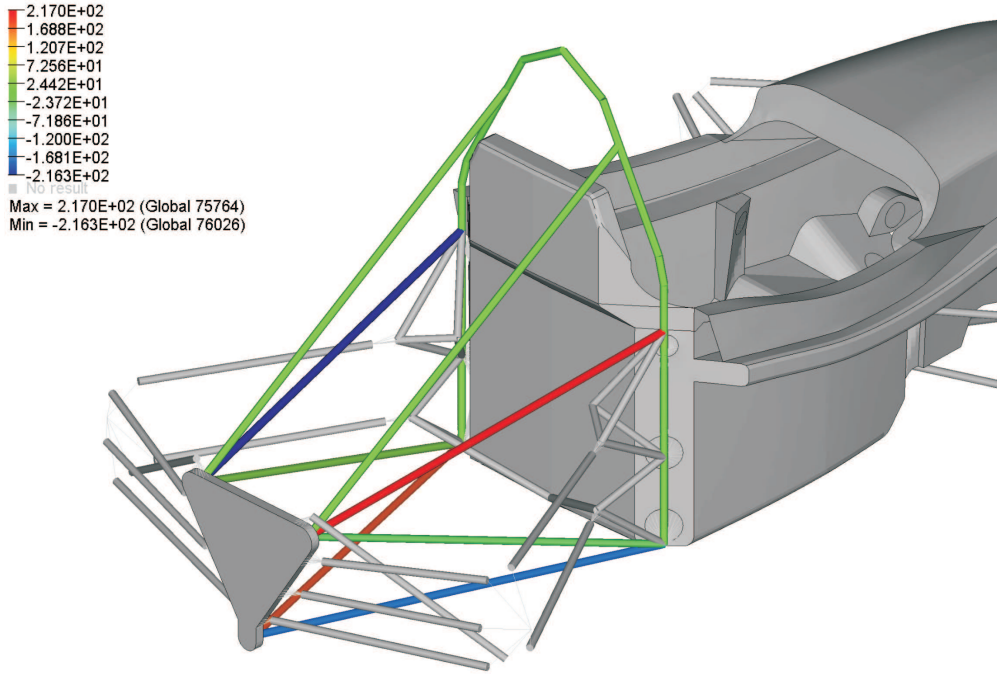


Figure 8.22: The stresses in the rear frame under torsional load

outer diameter $OD = 25$ mm with a wall thickness of $t = 1$ mm. Now looking at the stresses the maximum tensile and compressive forces are calculated and, assuming the tubes are loaded in pure tension and compression, they are evaluated for tensile and buckling strength. The maximum stress is approximately ± 300 N/mm 2 which for the given tube geometry results in a maximum force of 300 N/mm $^2 / 75.5$ mm $^2 = 22.5$ kN. Now the maximum tensile strength for mild steel ($\sigma_{max} = 350$ N/mm 2) is easily calculated by:

$$F_{tens_{max}} = \sigma_{max} \cdot A = 26.5 \text{ kN} \quad (8.1)$$

For the buckling strength we assume a maximum length of $L = 0.9$ mm at the tubes to be clamped at one end. For the maximum buckling force we can write:

$$F_{buck_{max}} = \frac{4\pi^2 EI}{L^2} = 45 \text{ kN} \quad (8.2)$$

With E the modulus of mild steel and $I = \pi/64 \cdot (OD^4 - (OD - t)^4)$ the tubular second moment of area. For the given material and geometry the frame would suffice. However one might consider to use slightly better steel to be on the safe side regarding tensile strength.

8.7 Front impact equivalency

Regarding the front impact support equivalence is determined with respect to a standard tubular frame, in addition it must be able to withstand 120 kN static force. A steel tubular frame would consist of 4 horizontal tubes in the forward direction while the monocoque is assumed to be a square section. For convenience only quarter A of the structure is evaluated as shown in Figure 8.23 which is assumed to have length $L = 500$ mm perpendicular to the drawing plane and is clamped at one side. The compressive strength and the modulus EI , determining bending and buckling strength, are calculated around the dotted line in quarter A and presented in Table 8.3. Note that for the monocoque only the faces are evaluated because $\sigma_{max_f} \gg \sigma_{max_c}$ and $E_f \gg E_c$. In addition because the maximum allowable stress for a laminate with different ply orientations is difficult to evaluate, only the surface area of one ply with $t_f = 0.2$ mm and tensile strength $X = 1550$ N/mm² is used to for comparison. To compare the bending/buckling strength the whole thickness $t_f = 1$ mm is used, with E_f the value from Table 8.2. In Table 8.3 is shown that equivalency is easily achieved for the front impact support as well as the 120 kN demand. For the second moment of area we can write for the tube and the monocoque respectively:

$$I_{tube} = \frac{\pi}{64}(DO^4 - DI^4) \quad (8.3)$$

$$I_{plate} = \frac{t_f(h_1^3 + h_2^3)}{12}$$

	Tensile strength: $\sigma_{max} \cdot A$	Bending/buckling modulus: EI	Buckling force: $4\pi^2EI/L^2$
tube	39 kN	$1.6 \cdot 10^9$ Nmm ²	250 kN
monocoque corner	240 kN	$68 \cdot 10^9$ Nmm ²	1100 kN

Table 8.3: Equivalency of one-fourth of the monocoque front bulkhead support

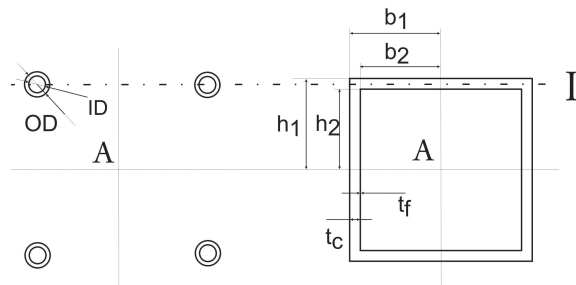


Figure 8.23: Simplified section cuts of the front impact support for a tubular frame and the monocoque, $h_1 = b_1 = 200$ mm, $h_2 = b_2 = 188$ mm, $t_c = 10$ mm, $t_f = 1$ mm, $OD = 25$ mm and $ID = 22$ mm

8.8 Side impact/front roll hoop bracing equivalency

The side impact structure in a tubular frame consists of 3 tubes as shown in Figure 2.3. A simplified drawing for the side impact is shown in Figure 8.24. The tubular is modeled as 3 horizontal tubes while the monocoque side impact is modeled as a plate with a rectangular rib on the surface. For the front roll hoop bracing a very similar analysis is made except that it consists of two tubes. Furthermore the monocoque shows a strongly curved plate where the front equivalency must be achieved. For convenience it is modeled as a plate with perpendicular edges. Analogous to section 8.7 the equivalent strength parameters are calculated and shown in Table 8.4. For the second moments of inertia we can now write:

$$\begin{aligned} I_{tube} &= \frac{\pi}{64}(DO^4 - DI^4) \\ I_{sideimpact} &= \frac{2h((\frac{1}{2}t_c + t_f)^3 - (\frac{1}{2}t_c)^3) + 2t_f b_r^3 + h_r((t_r + t_f)^3 - t_r^3)}{12} \quad (8.4) \\ I_{frontbracing} &= \frac{2h((\frac{1}{2}t_c + t_f)^3 - (\frac{1}{2}t_c)^3) + 2t_f(b_{s1}^3 + b_{s2}^3)}{12} \end{aligned}$$

	Tensile strength: $\sigma_{max} \cdot A$	bending/buckling modulus: EI
Tubular side impact	$3 \cdot 45 \text{ kN}$	$5.4 \cdot 10^9 \text{ Nmm}^2$
Monocoque side impact	260 kN	$6.4 \cdot 10^9 \text{ Nmm}^2$
Tubular front bracing	$2 \cdot 45 \text{ kN}$	$3.6 \cdot 10^9 \text{ Nmm}^2$
Monocoque front bracing	217 kN	$6.3 \cdot 10^9 \text{ Nmm}^2$

Table 8.4: Equivalency of the monocoque side impact and front bracing

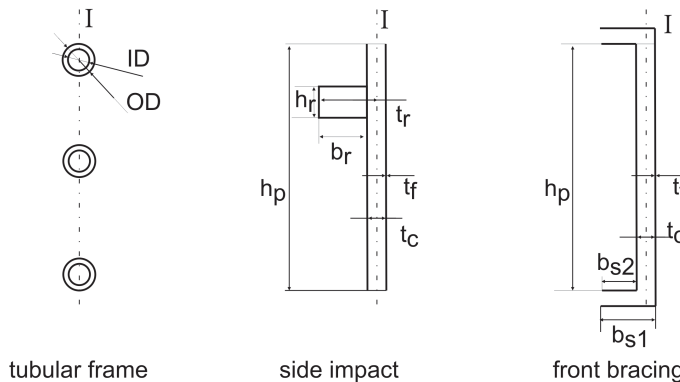


Figure 8.24: Sections cuts of a simplified tubular side impact/front bracing and equivalents in the monocoque, $h = 350 \text{ mm}$, $t_f = 1 \text{ mm}$, $t_c = 10 \text{ mm}$, $t_r = 55 \text{ mm}$, $b_r = b_{s1} = 75 \text{ mm}$, $b_{s2} = 63 \text{ mm}$, $h_r = 50 \text{ mm}$, $OD = 25 \text{ mm}$ and $ID = 21.5 \text{ mm}$

Chapter 9

Conclusions and Recommendations

This report describes the design of a lightweight, high stiffness, hybrid chassis consisting of a carbon fiber reinforced composite monocoque combining structural, esthetic, ergonomic and crash properties, and a steel tubular rear space frame.

The available materials have been evaluated and specifically the limitations and opportunities of engineering with fiber reinforced composites have been explored. They have been implemented in the monocoque design, keeping in mind the demands for high specific stiffness and strength. Stiffness and strength issues have also been approached from a pure structural design point of view, resulting in geometrical improvements of the chassis as a whole and the loading points in particular. The complex shapes required from monocoque cockpit designs with implemented structural, esthetic, ergonomic and crash properties are all combined in only four simple basic molds using the Multi-Shell Assembly Approach, making the chassis fairly simple to produce. Finally the monocoque has been optimized using global ply failure analysis to remove geometrical inefficiencies and the first eigen modes have been used to improve weak spots regarding specific stiffness. Also equivalency to a certain steel tubular frame regarding crash sensitive areas has been established. Furthermore the rear frame tube dimensions have been chosen such that a lightweight though stiff and strong tubular frame emerged, again using extensive FEA techniques.

The loading points in composite material structures are a field of expertise in their own. The variables in reducing the peak stresses around the hardpoints have been identified and suggestions have been made to reduce them. While extensive analysis has been done on these so called hard points and the effect of quite a few measures to reduce the stresses has been shown, testing is required to evaluate the results and prove that the strength targets are met.

Testing is also required when the car is finished, to evaluate the torsional stiffness analysis and to determine the overall mass and center of gravity height.

For future chassis designs one might want to consider to implement a carbon

fiber tubular rear frame or something equivalent. Analysis has shown that another 7 kg of weight can be saved on the rear frame alone. Crucial hereby is to design a method of efficiently bonding the carbon fiber tubes to each other and the other chassis components. For ideas one could look at the bicycle industry.

For the future I also strongly recommend to reevaluate the suspension system parallel to designing a new chassis. By good interaction of the two design processes a lot of difficult engineering issues could be prevented by making the suspension system and the chassis more compliant to one another, instead of having to work around a predesigned suspension system.

Appendix A

Why lightweight?

A lot of effort generally goes into the development of lightweight vehicles. A compromise must be found however between lightweight design and the cost that is paid to achieve this. A simplified vehicle model is used to analyse reasons for lightweight design. Besides the obvious benefit of lightweight design with respect to the power to weight ratio, the achievable cornering velocity is strongly determined by the C.O.G. height and vehicle mass.

A.1 The downside of load transfer

The main issue in vehicle dynamics is the load transfer that occurs during cornering, braking and accelerating. During cornering the outside tyres are more heavily loaded than the inside tyres due to a momentum that results from the lateral acceleration a_y (centrifugal force) of the car. The load is "transferred" from the inside to the outside tyres. While accelerating and decelerating the same holds for the rear and front tyres respectively. In Figure A.1 the forces are shown that act on a simplified two-wheel model of a cornering car. In this figure m is the vehicle mass, φ the roll angle, h the C.O.G. height and h_{rc} the roll center height. Roll center R has a stiffness c_φ . Note that this is just the front or rear axle, so in calculations half the vehicle mass is used, assuming a 50-50% weight distribution over the front and rear axle.

Load transfer results here in an increase in the left vertical tyre force F_{zL} and a decrease in F_{zR} by ΔF_z . The amount of lateral tyre force F_y that the two tyres generate together determines the amount of lateral acceleration that can be achieved i.e. how fast the car can get around a corner. Because F_y is simply the lateral friction coefficient μ_y times the vertical tyre force F_z , one would expect that the totally produced F_y remains equal, because the sum of F_{zL} and F_{zR} remains equal. This is however not the case. First of all the peak lateral friction coefficient μ_y of the tyres actually decreases for an increasing vertical tyre force. The influence of the vertical tyre force on the friction coefficient differs for each type of tyre. In Figure A.2a this effect is shown for the tyres used by URE (20.5x6-13 R25A Hoosier)¹.

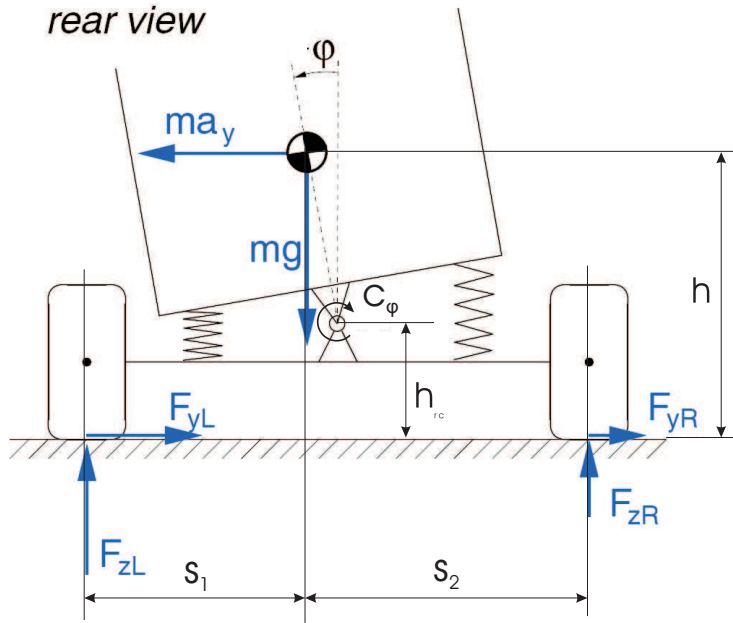


Figure A.1: The forces on a simplified two-wheel model with body roll

The total lateral force F_y produced by the two tyres equals [2]:

$$(F_{z1} - \Delta F)(\mu_{y1} + \Delta\mu) + (F_{z1} + \Delta F)(\mu_{y1} - \Delta\mu) = 2F_{z1}\mu_{y1} - 2\Delta F\Delta\mu \quad (\text{A.1})$$

The loss of produced lateral force then consists of : $2\Delta F\Delta\mu$.

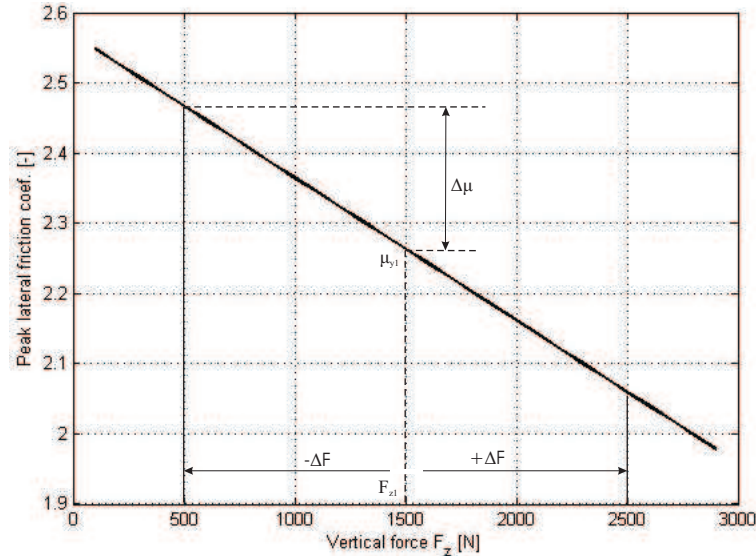


Figure A.2: The loss in peak lateral friction coefficient due to an increasing vertical tyre force

Appendix A. Why lightweight?

The second cause of loss in produced lateral force comes from the non-linear relation between the vertical tyre force F_z and the cornering stiffness $C_{f\alpha}$. The cornering stiffness determines the lateral tyre force F_y for small tyre side slip angles α as shown in Figure A.4. The loss of cornering stiffness due to an increase in load transfer is illustrated in Figure A.3. $C_{f\alpha}$ is shown for several small side slip angles showing the shift of the peak cornering stiffness down and to the right for increasing side slip angles. This means that for larger α , one suffers additional loss in generated lateral tyre force on top of the effect shown below.

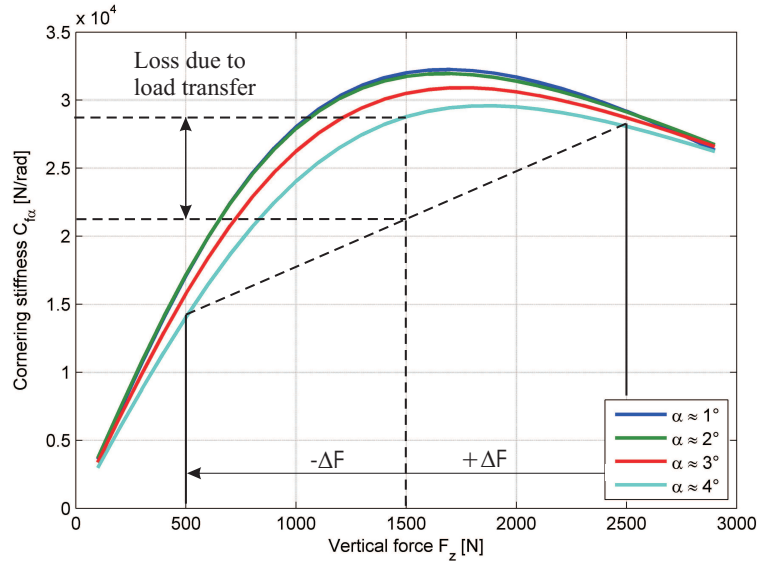


Figure A.3: The loss cornering stiffness $C_{f\alpha}$ due to an increasing vertical tyre force

¹Both the degressive friction coefficient and cornering stiffness have been analyzed for this specific tyre using the DELFT-TYRE module in MATLAB (www.delft-tyre.com)

A.2 Low and lightweight

The effects described above are the reasons why race cars are engineered to have a low C.O.G. At a certain point however further lowering the C.O.G. will become technically, financially and practically impossible given the circumstances. To find an optimum the effect of the C.O.G. height h and vehicle mass m on the amount of load transfer is calculated. Firstly the loss of produced lateral force ΔF_y is determined by looking at the left and right tyre forces as a function of the tyre side slip angle α and lateral vehicle acceleration a_y . This is compared to the situation where no load transfer would occur during cornering. Here a 250 kg car (incl. a 68 kg driver, currently 298 kg) with a C.O.G. height of 250 mm is analyzed. The analysis consists of a steady state cornering test, meaning that the longitudinal acceleration is assumed to be very small. Also dynamic effects resulting from sudden changes in the lateral acceleration are excluded. Looking at Figure A.4 one can see that for small α , thus small a_y , the cornering stiffness determines the lateral tyre force. For larger α the lateral friction coefficient becomes more important. Not surprisingly the difference in produced lateral force with and without load transfer increases for larger α , peaks at the point where the tyre starts slipping and then reduces again (Figure A.5a). Because this is the critical point, further analysis is executed with a tyre side slip angle *alpha* of 5°. The analysis includes lateral accelerations of up to 2 g, as can be seen from Figure A.5b, which is the maximum lateral acceleration a formula student race car experiences on a typical event track according to Dr Blake Siegler [17]. This is still a very high value for the lateral acceleration. Most of the time during cornering it will be nearer to 1 to 1,5 g.

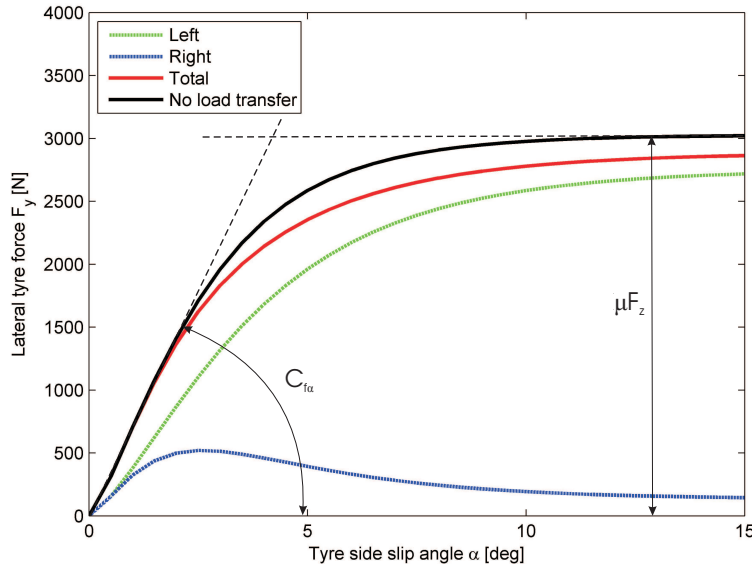


Figure A.4: Produced lateral tyre forces with and without load transfer ($m = 250$ kg, $h = 250$ mm)

It is clearly beneficial to minimize the amount of load transfer that occurs during cornering. From force and momentum equilibrium in Figure A.1 is derived

Appendix A. Why lightweight?

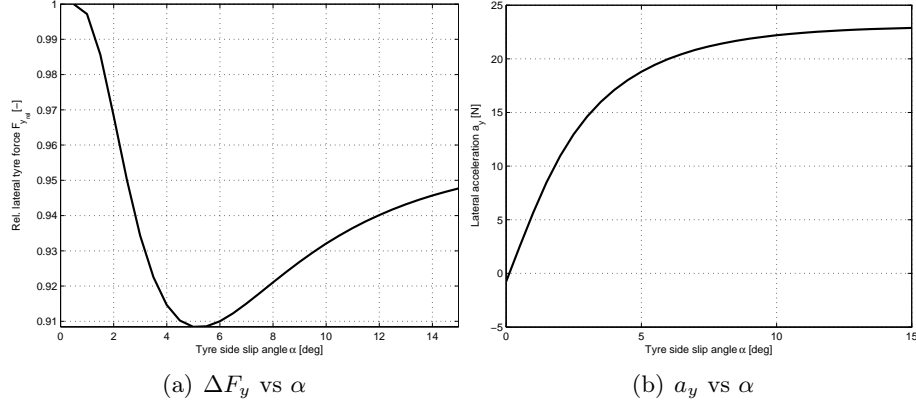


Figure A.5: Relation between the tyre side slip angle α and the lateral acceleration a_y and relative produced lateral F_y

that the load transfer and corresponding vehicle roll angle can be written as:

$$\begin{aligned} \Delta F_{z,roll} &= \frac{h_{rc}F_y + c_\varphi\varphi - F_z(\frac{1}{2}s_1 - \frac{1}{2}s_2)}{s_1 + s_2} \\ \varphi &= \frac{\frac{1}{2}ma_y(h - h_{rc})}{c_\varphi - \frac{1}{2}mg(h - h_{rc})} \end{aligned} \quad (\text{A.2})$$

Note that half the vehicle mass is used because of the simplified single axis analysis and equation A.2 only holds for small φ . So besides the vehicle mass m and the C.O.G. height h , the roll center height h_{rc} and the trackwidth $s_1 + s_2$ determine the amount of load transfer during cornering. The roll stiffness is indirectly of influence. It doesn't decrease the load transfer but the roll angle φ . Body roll increases s_1 (C.O.G. shifts to the left), increasing the load transfer, so a larger roll stiffness does decrease ΔF_y . The change of h due to body roll is neglected because of the small roll angles.

Appendix B

Cockpit regulations

Regarding safety, a driver must be able to egress from the cockpit very easily. For this reason some very demanding rules have been stated for the cockpit dimensions. A horizontal profile of the shape shown in Figure ??a must be able to fit into the cockpit opening to a height of 350 mm above the ground. In addition a profile of the shape shown in Figure B.1b must fit through the cockpit forwards in vertical position right up to the pedalbox.

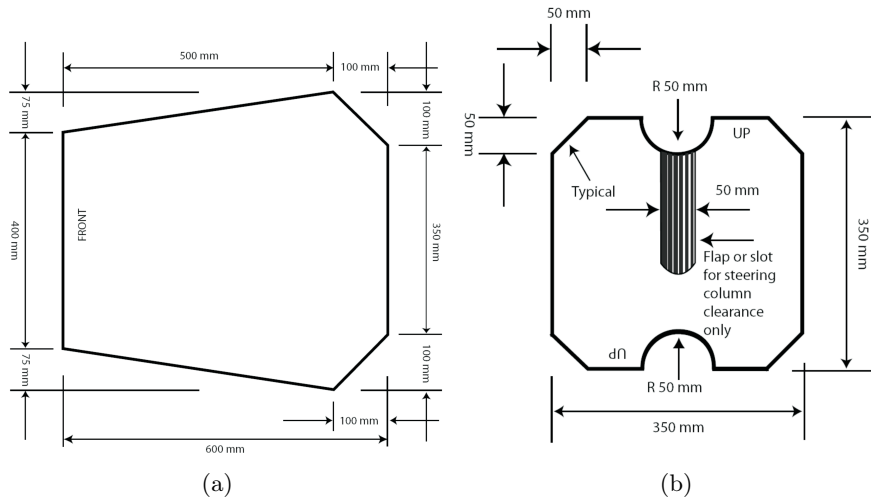


Figure B.1: Minimal cockpit dimensions

Bibliography

- [1] 2008 *Formula SAE Rules*. 2007.
- [2] I.J.M. Besselink. *Lecture notes 2005/2006/2007 Vehicle Dynamics 4L150*. 2005.
- [3] Andrew Deakin; David Crolla *et al*. The effect of chassis stiffness on race car handling balance. *Society of Automotive Engineers, Inc.*
- [4] Choon Chiang Foo; Gin Boay Cha *et al*. Mechanical properties of nomex material and nomex honeycomb structure. *Elsevier: Composite Structures 80* (2007) 588–594.
- [5] Elena Bozhevolnaya; Anders Lyckegaard *et al*. Structurally graded core inserts in sandwich panels. *Composite Structures 68*(2005) pg. 23-29.
- [6] Elena Bozhevolnaya; Anders Lyckegaard *et al*. Local effects in the vicinity of inserts in sandwich panels. *Elsevier Composites: Part B 35* (2004) pg. 619-627, 2003.
- [7] Elena Bozhevolnaya; Ole.T. Thomson *et al*. Local effects across core junctions in sandwich panels. *Elsevier Composites: Part B 34* (2003) pg. 509-517.
- [8] Kohei Ichikawa; Yuichiro Shin *et al*. A three-dimensional finite-element stress analysis and strength evaluation of stepped-lap adhesive joints subjected to static tensile loadings. *International Journal of Adhesion and Adhesives 28* (2008) 464–470.
- [9] Ole Thybo Thomsen; Elena Bozhevolnaya *et al*. Structurally graded core junctions in sandwich elements. *Elsevier Composites: Part A 36* (2005) 1397–1411.
- [10] Weidner; L. R. Radford *et al*. A multi-shell assembly approach applied to monocoque chassis design. *SAE CONFERENCE PROCEEDINGS P*, 2002, ISSUE 382, pages 747-752.
- [11] M.G.D. Geers. *Applied Elasticity in Engineering, lecture notes*. Eindhoven University of Technology, Faculty of Mechanical Engineering, Computational and Experimental Mechanics.
- [12] William B. Riley; Albert R. George. Design, analysis and testing of a formula sae car chassis. *Proceedings of the 2002 SAE Motorsports Engineering Conference and Exhibition*, 2002.

Bibliography

- [13] Isaac M. Daniel; Ori Ishai. *Engineering mechanics of composite materials*. Oxford University Press, 1994.
- [14] M.P. Koster. *Constructieprincipes voor het nauwkeurig bewegen en positioneren*. Twente University Press, Enschede, 3e herziene druk 2000.
- [15] Willem-Jan Lamers. Development and analysis of a multi-link suspension for racing applications. 2008.
- [16] A.C.C.M. Oomen. Toepassen van vezelversterkte kunststoffen in een wedstrijdroeiboot.
- [17] Dr. Blake Siegler. *Formula Student Event Track Data*. 1999.
- [18] a Gurit brand SP. *Guide to composites*.
- [19] Andries van Berkum. Chassis an suspension design fsrteo2. 2006.